The Journal of Physiology

Impacts of perinatal nicotine exposure on nicotinic acetylcholine receptor expression and glutamatergic synaptic transmission in the mouse auditory brainstem

Mackenna Wollet, PhD[1], Abram Hernandez[1], Kaila Nip, MS[1], Brett Ginsburg, PhD[2], Jason R. Pugh, PhD[1] and Jun Hee Kim, PhD[1,3]

[1]*Department of Cellular and Integrative Physiology, UT Health San Antonio, San Antonio, Texas, USA*
[2]*Department of Psychiatry and Behavioral Science, UT Health San Antonio, San Antonio, Texas, USA*
[3]*Department of Otolaryngology and Cell and Developmental Biology, Kresge Hearing Research Institute, University of Michigan, Ann Arbor, Michigan, USA*

Handling Editors: David Wyllie & Conny Kopp-Scheinpflug

The peer review history is available in the Supporting Information section of this article (https://doi.org/10.1113/JP286971#support-information-section).

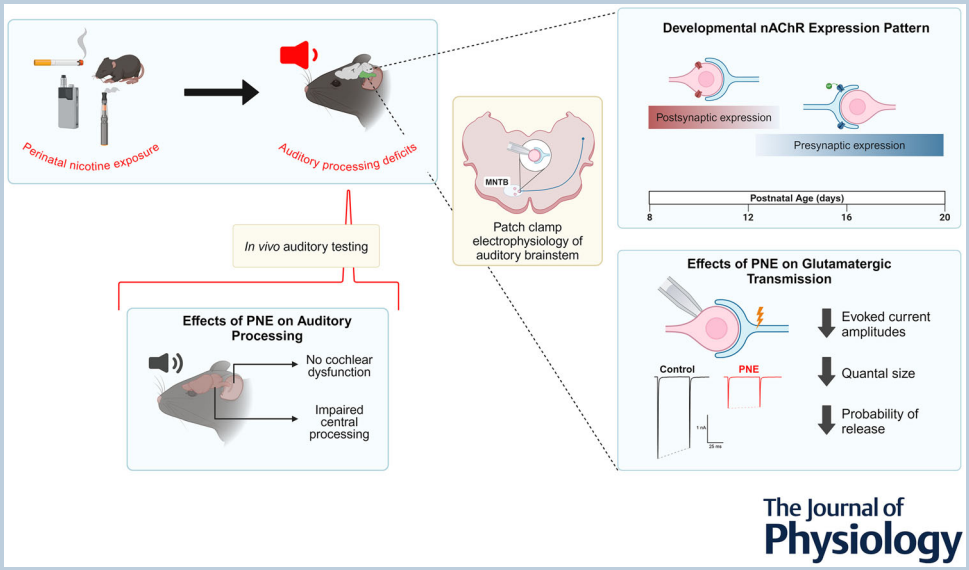

Abstract figure legend Developmental nicotine exposure is known to cause a myriad of health defects including auditory processing deficits. In human and animal studies, nicotine exposure can lead to impaired auditory temporal processing and disrupted glutamate synapse development within the auditory cortex. Nicotinic acetylcholine receptors (nAChRs) are distributed across the auditory pathway, and recent work demonstrates cholinergic influence on MNTB neurons. As a key synapse for sound localization computations, we sought to investigate how perinatal nicotine exposure (PNE) might affect the development of the calyx of Held-MNTB cell synapse and ultimately how PNE impairs auditory processing. We observed temporal and subcellular localization patterns of nAChR expression within the MNTB which is disrupted by PNE. PNE also impairs glutamatergic transmission at the calyx synapse and causes deficits in central auditory processing without affecting cochlear function. These results suggest that PNE disrupts nAChR patterning that is important for proper MNTB development and auditory processing.

DOI: 10.1113/JP286971

Abstract *In utero* nicotine exposure from maternal smoking is linked to increased risk of auditory processing deficits. This study investigated the impact of developmental nicotine exposure during the critical period on nicotinic acetylcholine receptor (nAChR) functional expression, glutamatergic synaptic transmission and auditory processing in the mouse auditory brainstem. We assessed nAChR function at a central synapse and the consequences of perinatal nicotine exposure (PNE) on synaptic currents and auditory brainstem responses (ABRs) in mice. Our results indicate developmentally regulated changes in nAChR expression in medial nucleus of the trapezoid body (MNTB) neurons and presynaptic calyx of Held terminals. PNE led to increased ACh-evoked postsynaptic currents and impaired glutamatergic neurotransmission, underscoring the importance of nAChR activity in early auditory synaptic development. PNE also increased ABR thresholds and reduced ABR peak amplitudes, indicating impaired central auditory processing without cochlear dysfunction. Our study provides new insights into the synaptic disruptions underlying auditory deficits from prenatal nicotine exposure.

(Received 22 May 2024; accepted after revision 24 March 2025; first published online 30 April 2025)
Corresponding author Jun Hee Kim: Department Otolaryngology and Cell and Developmental Biology, Kresge Hearing Research Institute, University of Michigan, Ann Arbor, Michigan, USA. Email: kimjunh@med.umich.edu

Key points

- *In utero* nicotine exposure leads to increased risk of sensory processing deficits and elevated expression of nicotinic acetylcholine receptors (nAChRs).
- nAChRs are essential for auditory processing and are present in the auditory brainstem.
- Within the medial nucleus of the trapezoid body in the auditory brainstem, the patterning of nicotinic receptor expression during development and how nicotine exposure might affect this are unknown.
- Nicotinic receptors are expressed postsynaptically before hearing onset and switch to presynaptic expression after hearing onset.
- Perinatal nicotine exposure disrupts physiological nicotinic receptor patterning and impairs synaptic transmission at the calyx of Held.

Introduction

Prenatal nicotine exposure, resulting from maternal smoking during pregnancy, has been shown to cause a range of long-term neurodevelopmental defects in children (Crane et al., 2009; Ghanizadeh, 2011; Katbamna et al., 2013; King et al., 2018; Marco et al., 2011), including attention-deficit disorder and learning disabilities, which are shown to be comorbid with sensory processing deficits (Crane et al., 2009; Ghanizadeh, 2011; Marco et al., 2011). Due to the increased prevalence of electronic cigarettes, this requires the need for investigation into the effects of prenatal exposure to nicotine alone on fetal health and development (Kramarow & Elgaddal, 2023). *In utero* nicotine exposure can cause hearing impairments and auditory processing disorders leading to speech and language delays, poor sound localization and difficulty understanding speech in noisy environments (King et al., 2018). Animal studies have demonstrated that nicotine exposure during development impairs temporal processing in an auditory startle test and disrupts the development of glutamatergic synapses in the auditory

Mackenna Wollet received her PhD under the mentorship of Drs Jun Hee Kim (University of Michigan) and Jason R. Pugh (UT Health San Antonio) in October 2024 from UT Health San Antonio. As an undergraduate Mackenna began her research journey in the laboratory of Dr Michael Beckstead where she learned patch-clamp electrophysiology in dopamine neurons within the ventral tegmental area. She found herself drawn to slice-level neurophysiology and joined the laboratory of Dr Jun Hee Kim in 2019 where she studied synaptic physiology in the MNTB of the auditory brainstem. Mackenna will continue her work in the world of auditory neuroscience as a postdoctoral fellow.

cortex (Aramakis et al., 2000; Sun et al., 2008). Nicotine is known to bind to and activate nicotinic acetylcholine receptors (nAChRs), which are widely distributed throughout the auditory nervous system and play a key role in synaptic transmission (Aramakis & Metherate, 1998; Beebe et al., 2021; Zhang et al., 2021). However, the specific effects of developmental nicotine exposure on nAChR signalling and auditory processing are not yet fully understood. In this study, we aim to investigate the impact of nicotine exposure during early development on auditory brainstem nAChR signalling, synaptic transmission, and auditory processing.

nAChRs are expressed throughout the auditory system and play a crucial role in auditory processing. These receptors are found on several peripheral and central auditory cells. Within the cochlea, $\alpha 9$ nAChRs are expressed on postsynaptic outer hair cells receiving cholinergic medial olivocochlear efferent terminals (Elgoyhen et al., 2009). In the auditory brainstem, nAChR expression has been demonstrated using receptor autoradiography, *in situ* hybridization, and immunohistochemistry of rodent cochlear nucleus, superior olivary complex (SOC), and inferior colliculus (Happe & Morley, 1998, 2004; Yao & Godfrey, 1999). Additionally, recent studies have confirmed the presence of nAChRs across all layers of the auditory cortex (Aramakis & Metherate, 1998; Ghimire et al., 2020), where cholinergic modulation of neuronal activity enhances responses to auditory inputs (Chen & Yan, 2007; Metherate et al., 2012). In the inferior colliculus, $\alpha 3\beta 4$ nAChRs, a rarer nAChR subtype, play a role in regulating the excitability of VIP neurons (Rivera-Perez et al., 2021). Moreover, *in vivo* recordings of the MNTB showed that nAChRs play a critical role in regulating tone-evoked activity and accurately coding signal-in-noise detection (Zhang et al., 2021). In addition to nAChR expression, muscarinic acetylcholine receptors modulate the excitability of MNTB principal neurons before hearing onset (Weimann et al., 2024).

In terms of subcellular location at central synapses, nAChRs can be located on both pre- and postsynaptic domains to regulate neurotransmission. For example, presynaptic $\alpha 7$ nAChRs increase glutamate release to enhance N-methyl-D-aspartate receptor (NMDAR)-mediated excitatory postsynaptic potentials (EPSPs) in apical dendrites of pyramidal neurons in the developing auditory cortex, and this effect is eliminated by postnatal day 21 (p21) (Aramakis & Metherate, 1998). This transient effect highlights the importance of nAChRs during the critical period of development in the auditory cortex, suggesting the role in glutamatergic synapse maturation. Postsynaptic nAChR expression in neurons of the ventral nucleus of the lateral lemniscus (VNLL) is observed before hearing onset and subsequently declines with age (Baumann & Koch, 2017). Despite the importance of nAChR expression at local synapses during auditory development, the cellular mechanisms by which nicotine exposure during early postnatal development alters synaptic transmission at the level of a single synapse remain unclear.

The calyx of Held-MNTB synapse is a very reliable synapse with high temporal precision that allows for binaural sound localization computations in the auditory brainstem. Studies utilizing autoradiography techniques have demonstrated the dynamic expression pattern of nAChRs in the MNTB, which is high during the second postnatal week, typically considered the critical period of auditory development (Happe & Morley, 2004). Concurrently, PNE impairs the development of glutamatergic inputs and temporal precision of action potential firing in the VNLL within the auditory brainstem (Baumann & Koch, 2017).

In this study, we employed a perinatal nicotine exposure (PNE) model that subjects neonatal pups to nicotine (postnatal days 8–12) to investigate the effects of developmental nicotine exposure during the critical period similar to the fetal *in utero* condition. Utilizing *ex vivo* and *in vivo* electrophysiology in this model, we aim to study the impact of PNE on the developmental processes of auditory synapses within the auditory brainstem. Specifically, we focus on investigating the functional expression of nAChRs within the calyx of Held-MNTB synapse during the postnatal period and delineating how PNE perturbs the developmental dynamics of nAChRs and the maturation of glutamatergic transmission. By elucidating the cellular mechanisms whereby PNE impact auditory brainstem development and processing, this research contributes to uncovering potential therapeutic targets and interventions aimed at ameliorating the adverse effects of PNE on auditory function.

Materials and methods

Animals

Both sexes of C57BL/6J mice ($n = 114$ total) were used according to the guidelines approved by the UT Health San Antonio Institutional Animal Care and Use Committee. All experiments were performed between postnatal days 8 and 24 during the animals' light cycle. Animals were housed in a 12-h light–dark cycle with *ad libitum* access to food and water.

PNE protocol

Our PNE protocol utilized subcutaneous injections of nicotine hydrogen tartrate (0.7 mg/kg free base nicotine) dissolved in 0.9% sterile saline to pups on postnatal days 8–12 twice daily (totalling 1.4 mg/kg/day). Littermate

controls were injected with comparable volumes of saline vehicle. Pups were taken from the home cage for injections and monitored for 15 min post injection before being returned to their home cage. This dosage has been used previously to study chronic nicotine effects on the brain, and on the auditory system specifically, to approximate blood levels of nicotine in smokers (Abdulla et al., 1996; Aramakis et al., 2000; Liang et al., 2006; Rowell & Li, 2002).

Measurement of nicotine, cotinine and 3 hydroxy cotinine in plasma using liquid chromatography-tandem mass spectrometry

Standards nicotine (NIC), cotinine (COT) and 3 hydroxy cotinine (3OH COT) and the internal standards nicotine D4 (NIC D4), cotinine D3 (COT D3) and 3 hydroxy cotinine D3 (3OH COT D3) were purchased from Milli-Pore Sigma (St. Louis, MO, USA). All other HPLC-grade reagents were purchased from Fisher Scientific (Waltham, MA, USA). Milli-Q water was used for the preparation of all solutions. Super stock solutions of NIC, COT and 3OH COT were prepared in methanol at a concentration of 1 mg/ml and stored in aliquots at −80°C. A working stock solution of each drug was prepared daily from the super stock solutions at a concentration of 100 µg/ml and used to spike the calibrators.

The liquid chromatography-tandem mass spectrometry (LC/MS/MS) system consisted of a Shimadzu SIL-40C XR autosampler, two LC-40B XR pumps and a Shimadzu 8045 mass spectrometer. An ACE Excel C18 LC analytical column (75 × 3.0 mm, 3µm) was purchased from Mac-Mod Analytical (Chaddsford, PA, USA) and maintained at 24°C during the chromatographic runs using a Shimadzu CTO-40S column oven. The isocratic mobile phase consisted of 90% water and 10% isopropanol with 10 mM ammonium acetate, pH 6.9. The flow rate of the mobile phase was 0.4 ml/min with a 4-min run time. All the drugs were detected in positive mode with the following transitions: 163 > 130 NIC, 177 > 80 COT, 193 > 80 3OH COT, 167 > 136 NIC D4, 180 > 80.1 COT D3 and 196 > 80.15 3OH COT D3.

Calibrator samples were prepared daily by spiking blank plasma to obtain final concentrations of 0, 1, 5, 10, 50 and 100 ng/ml. Briefly 0.1 ml of the calibrator and unknown plasma samples were mixed with 10 µl of 10 µg/ml NIC D4, COT D3 and 3OH COT D3 and 0.5 ml of HPLC-grade isopropanol. The samples were vortexed vigorously for a minute and then centrifuged at 17,000 *g* for 5 min. The supernatants were transferred to new microcentrifuge tubes and dried to residue under a warm stream of nitrogen. The residue was then redissolved in 50 µl of the mobile phase, vortexed for 30 s and centrifuged for 2 min at 17,000 *g*. The samples were transferred to injection vials, and 10 µl was injected into the LC/MS/MS system. The ratio of each drug's peak area to its respective internal standard peak area for each unknown sample was compared against a linear regression of the ratios obtained by the calibration samples to quantify each drug. The concentration of COT and 3OH COT was expressed as ng/ml plasma (Fig. 4*B*).

Ex vivo brain slice electrophysiology

Slice preparation. Animals were deeply anaesthetized with isoflurane and quickly decapitated for brain slice collection. Brains were immediately removed and immersed in ice-cold low-calcium ACSF containing (in mM) 125 NaCl, 2.5 KCl, 3 $MgCl_2$, 0.1 $CaCl_2$, 25 glucose, 25 $NaHCO_3$ and 1.25 NaH_2PO_4, at pH 7.4 and osmolarity 310–320 mOsm, bubbled with carbogen (95% O_2, 5% CO_2). Transverse 200 µm-thick brainstem slices containing the MNTB were collected using a Vibratome (VT1200S, Leica, Wetzlar, Germany). After the slices were collected, they were placed in an incubation chamber containing 'reserve' ACSF bubbled with carbogen at 35°C for 30 min and then kept at room temperature for the remainder of the day. Reserve ACSF contains (in mM) 100 NaCl, 2.5 KCl, 2 $MgCl_2$, 1 $CaCl_2$, 25 glucose, 30 sucrose, 25 $NaHCO_3$ and 1.25 NaH_2PO_4 with similar pH and osmolarity to low-calcium CSF.

Electrophysiological recordings. Whole-cell patch-clamp recordings were performed in room-temperature normal ACSF, which consisted of the same components as low-calcium ACSF except that it contained 1 mM $MgCl_2$ and 2 mM $CaCl_2$. Reagents utilized externally (in ACSF) and internally (pipette solution) for each experiment are described. The analysis shown in Fig 1–5 used K-gluconate-based internal which contains (in mM) 125 K-gluconate, 20 KCl, 5 Na_2-phosphocreatine, 10 HEPES, 4 Mg-ATP, 0.2 EGTA and 0.3 GTP, pH adjusted to 7.3 with KOH osmolarity at 290 mOsm. The analysis in Fig. 6 used Cs-methane-sulfonate-based internal which contains (in mM) 130 Cs-methane-sulfonate, 10 CsCl, 5 EGTA, 10 HEPES, 4 ATP, 0.3 GTP, 5 Na_2-phosphocreatine, 10 TEA-Cl and 2 QX 314 with osmolarity at 290 mOsm. Glass capillaries were pulled using a Model P-1000 Micropipette Puller (Sutter Instruments, Novato, CA, USA) to obtain the tip resistance at 3–6 MΩ. Voltage-clamp and current-clamp experiments were performed using an EPC-10 amplifier (HEKA Elektronik, Lambrecht, Pfalz, Germany). For postsynaptic voltage clamp experiments holding potential was −65 mV. Series resistance (SR) was <20 MΩ without compensation, and if SR was >20 MΩ, compensation up to 50% was utilized. Any cell with a series resistance >40 MΩ was excluded from analysis. For current-clamp experiments junction

potentials were not corrected for. All miniature EPSC (mEPSC) recordings had TTX (0.5 μM) and atropine (1 μM) externally, and calcium-free mEPSC experiments had 0 mM $CaCl_2$ and 4 mM $MgCl_2$ externally. Acute puff application of ACh (1 mM) was performed with manual pressure using a 1 ml syringe for 1 s, and, for the experiment in Fig. 2, using a Pneumatic Drug Ejection System (npi Electronic Instruments, Tamm, Germany) (10 psi for 500 ms). In the analysis shown Fig. 2, postsynaptic pharmacology experiments utilized nAChR antagonists dihydro-β-erythroidine hydrobromide (DHβE, 3 μM, Tocris, Minneapolis, MN, USA) and methyllycaconitine (MLA, 10 nM, Tocris, Minneapolis, MN, USA). Drugs were bath-applied for 9 min before second puff application of ACh (4 min for drug to reach bath, then drug in contact with slice for 5 min). When MLA was utilized for the analysis shown in Fig. 3, 10 nM MLA was in the external ACSF for the entirety of recording experiments. For evoked EPSC (eEPSC) recordings, electrical stimulation was generated using a bipolar stimulating electrode placed

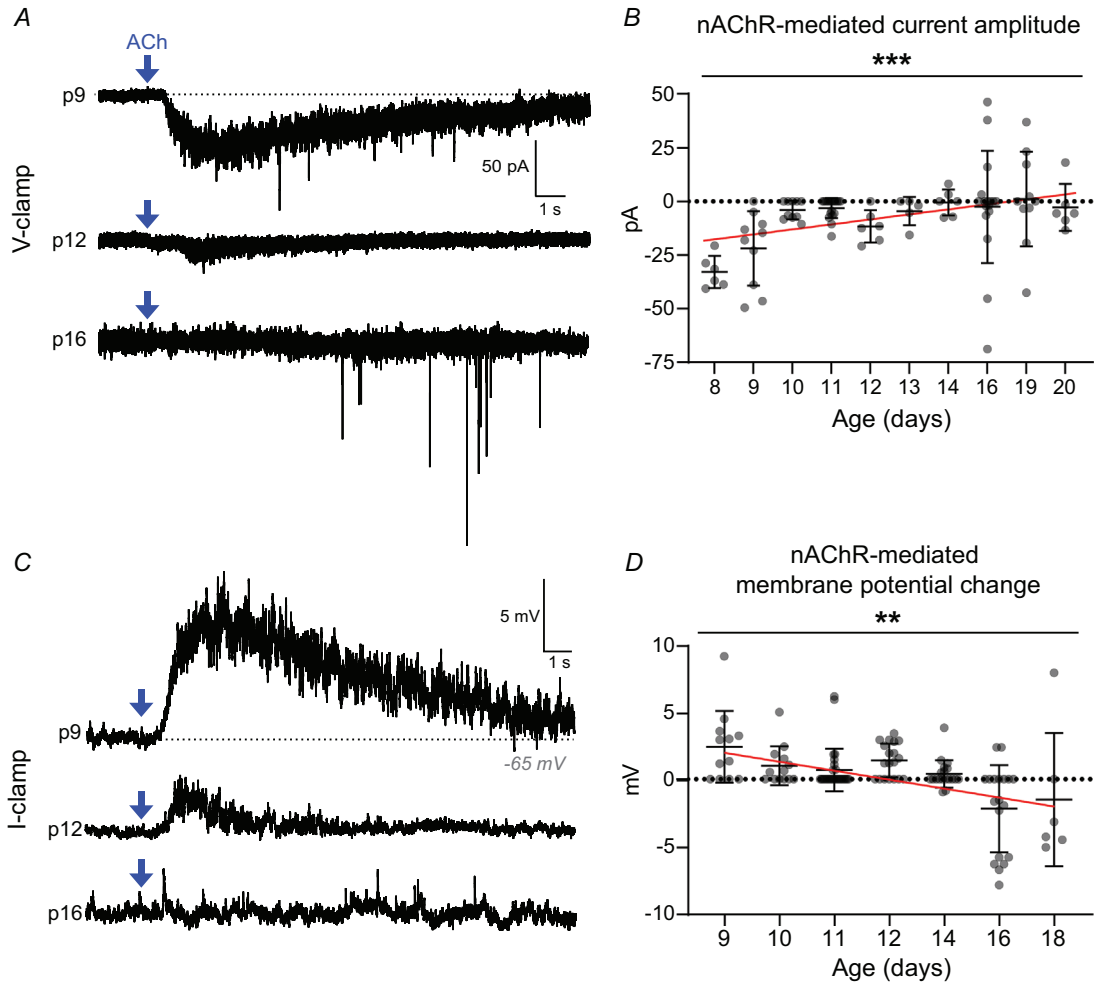

Figure 1. Age-dependent decrease in nAChR (nicotinic acetylcholine receptor) functional expression in MNTB principal neurons during postnatal development
A, representative current traces illustrating nAChR-mediated responses in MNTB neurons at postnatal day 9 (p9), p12 and p16, recorded using voltage clamp configuration (holding potential at −65 mV). ACh puffs (1 mM, 1 s) were administered at the timepoints denoted by blue arrows. *B*, scatter plot showing the amplitude of nAChR-mediated currents as a function of postnatal age up to p20. Each data point represents an individual neuron. A significant age-related decline in the amplitude of nAChR-mediated currents was observed (P = 0.000189, one-way ANOVA, n = 6–18 cells/timepoint). Simple linear regression slope (red) is significantly non-zero (t test, P = 0.0263). *C*, representative traces depicting changes in the membrane potential of MNTB neurons in response to ACh puffs at p9, p12 and p16. *D*, Quantitative analysis of membrane potential changes, determined by calculating the difference between resting potential and peak potential after acute ACh application. ACh-evoked depolarization was found to be significantly reduced up to p18 (P = 0.00286, one-way ANOVA, n = 6–29 cells/timepoint). Simple linear regression slope is significantly non-zero (t test, P = 0.00550). All quantitative data are presented as mean ± SD. [Colour figure can be viewed at wileyonlinelibrary.com]

at mid-line. After the threshold voltage of the stimulator was determined to elicit eEPSC, no more than 140% of threshold strength was used for the duration of the recording. eEPSC recordings contained strychnine (2 μM) and bicuculline (20 μM) in the external solution.

Electrophysiological data analysis. Whole-cell recordings were collected using PatchMaster and exported to Igor Pro 8 (Wavemetrics, Lake Oswego, OR, USA) for analysis. For acute puff experiments, no more than four cells were recorded from each slice (alternating recordings

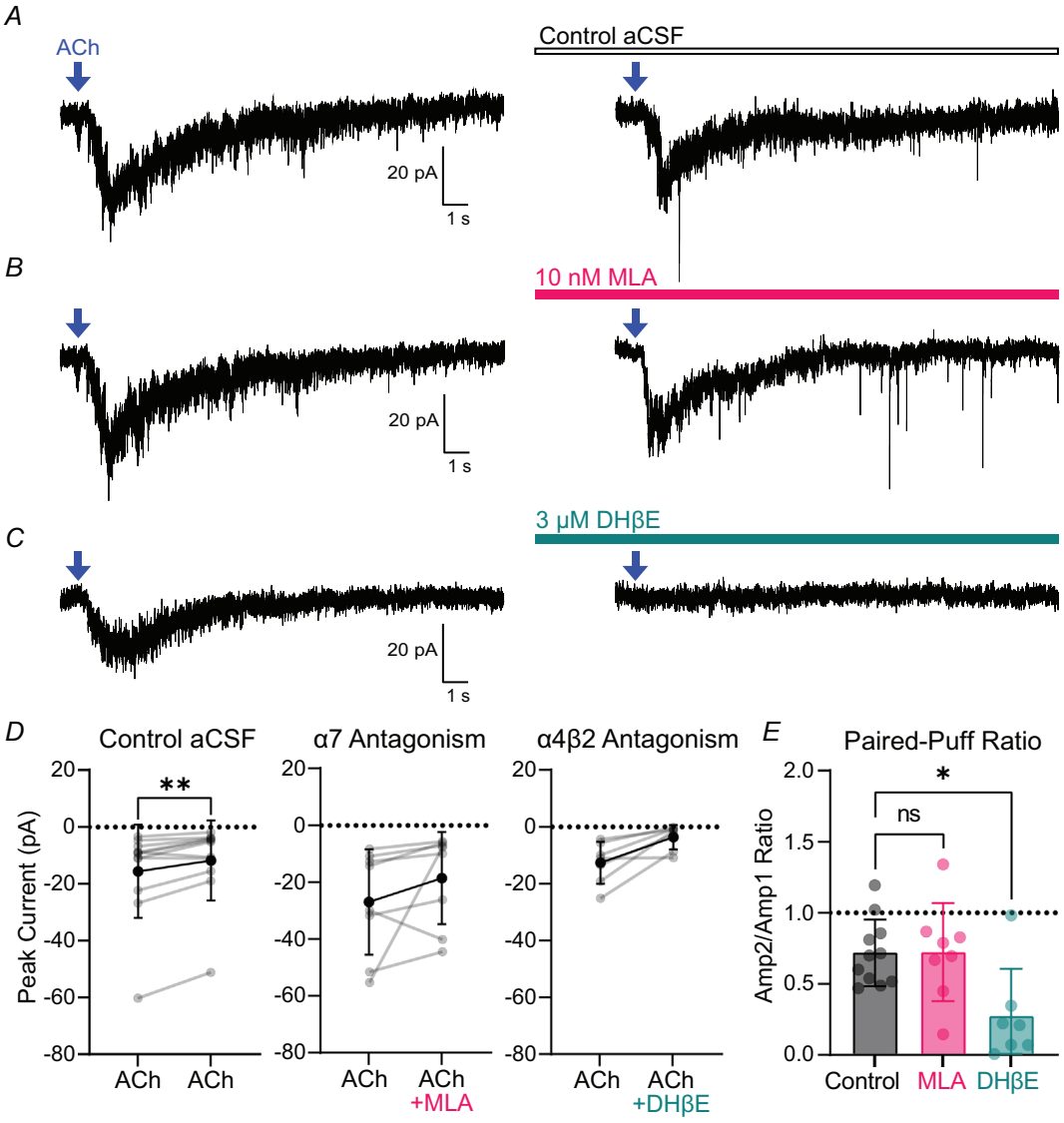

Figure 2. $\alpha 4\beta 2$ nAChRs (nicotinic acetylcholine receptor), not $\alpha 7$ nAChRs, mediate postsynaptic nAChR currents in pre-hearing MNTB principal neurons
Experimental design is utilized in this artwork. First puff application of ACh at 0 min followed by onset of bath application of either control ACSF or ACSF containing selective nAChR antagonist at 4 min. Second puff application of ACh was performed at 9 min. *A–C*, representative traces of postsynaptic ACh-evoked currents at p9–p10 in presence of atropine. ACh puff is denoted by a blue arrow. Traces on right are second ACh puff applications with control ACSF or nAChR antagonist bath-applied. *D*, quantification of ACh-evoked currents pre- and post-bath application of drug. Individual data points are shown in grey, and mean ± SD is shown in black. In control ACSF the first ACh-evoked current amplitude was significantly larger than the second (paired *t* test, n = 11 cells, P = 0.0043). *E*, the paired-puff ratio was calculated as follows: $\frac{\text{Current amplitude from second puff (Amp2)}}{\text{Current amplitude from first puff (Amp1)}}$. There was a significant effect of drug treatment on paired-puff ratio (P = 0.017, F = 4.78). Using Dunnett's multiple comparisons test DHβE (dihydro-β-erythroidine hydrobromide) had a significantly smaller paired-puff ratio compared to control (P = 0.015), whereas MLA (methyllycaconitine) was not significantly different from control (P = 0.89). [Colour figure can be viewed at wileyonlinelibrary.com]

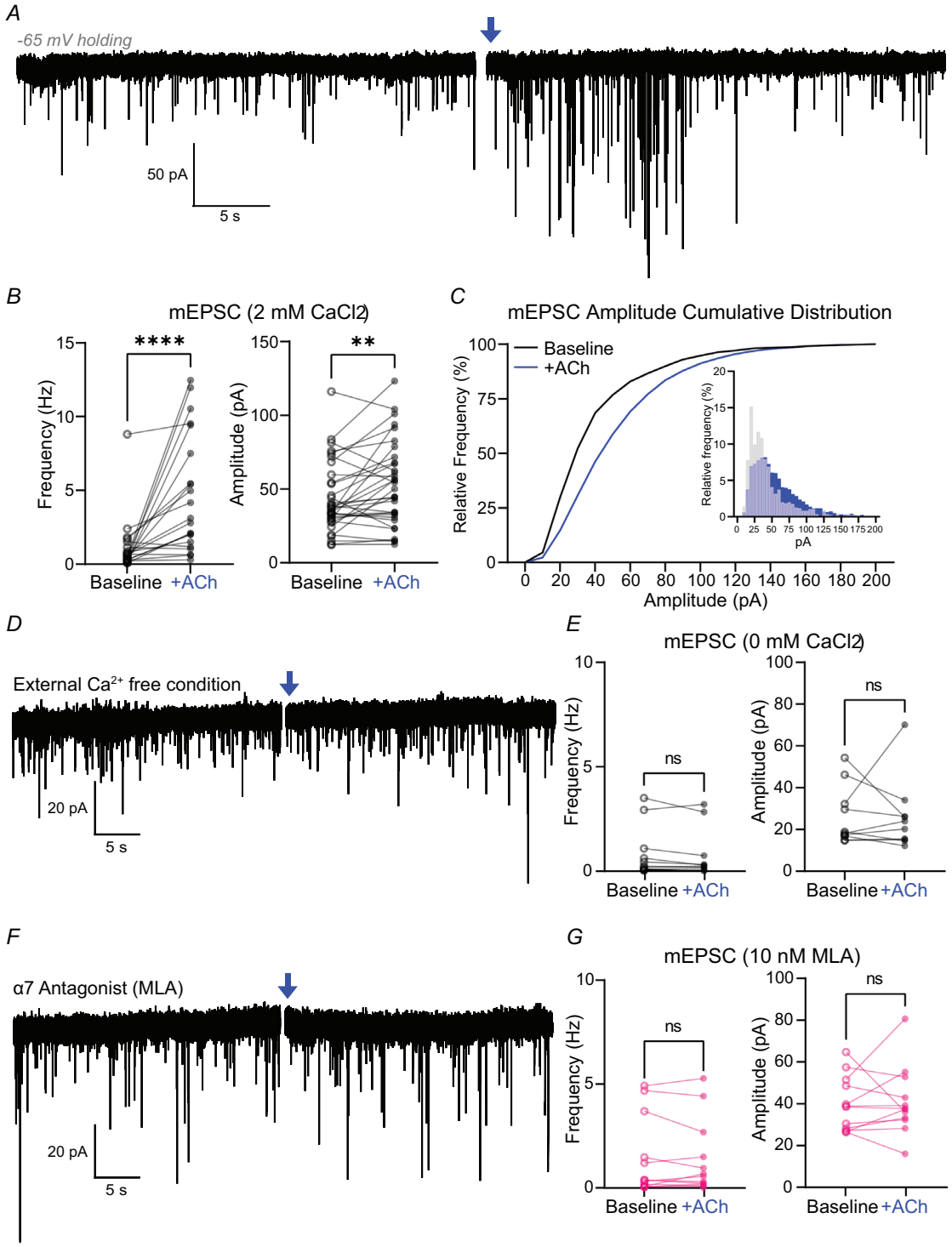

Figure 3. Activation of nAChR (nicotinic acetylcholine receptor) enhances vesicular glutamate release from the calyx of Held terminal
A, representative trace of mEPSCs in an MNTB neuron (at p16) in presence of TTX (0.5 μM). ACh puff application denoted by a blue arrow. *B*, mEPSC frequency and amplitude were quantified 30 s before (baseline, black) and immediately after ACh application (+ACh, blue). After ACh application, there was a significant increase in frequency (Wilcoxon matched pairs rank test, $P < 0.0001$, $n = 32$ cells) and amplitude (paired *t* test, $P = 0.007$, $n = 33$ cells). *C*, cumulative frequency distribution of mEPSC amplitudes at baseline and after ACh application. Inset:

frequency histogram showing mEPSC amplitudes. *D*, representative traces of mEPSCs in calcium-free external solution. *E*, quantification of mEPSC frequency and amplitude before and after ACh application in calcium-free external solution. There was no significant difference in frequency (P = 0.16, n = 11 cells) or amplitude (P = 0.69, n = 10 cells) using Wilcoxon matched pairs test. *F*, Representative traces of mEPSCs in presence of MLA (methyllycaconitine), an α7 nAChR antagonist. *G*, quantification of mEPSC frequency and amplitude before and after ACh application in presence of MLA. No significant difference was observed post-ACh puff in frequency (P = 0.71, n = 13 cells) or amplitude (P = 0.79, n = 12 cells) using paired t tests. [Colour figure can be viewed at wileyonlinelibrary.com]

with contralateral MNTB) to avoid desensitization of nAChRs. For mEPSC analysis, 30 s of activity pre- and post-ACh application was analysed per cell using Mini Analysis (Synaptosoft). For eEPSCs an average of five traces for single- and paired-pulse protocols was analysed per cell. 100 Hz trains were the averages of two to three traces for analysis. Probability of release (P_r) and readily releasable pool (RRP) estimates were calculated using the Schneggenburger–Meyer–Neher (SMN) method (Schneggenburger et al., 1999).

***In vivo* auditory testing.** Auditory testing occurred in a sound-attenuated chamber (Med Associates, Albans, VT, USA), with mice anaesthetized with isoflurane (Vet One, Boise, ID, USA) levels controlled by a Vapomatic

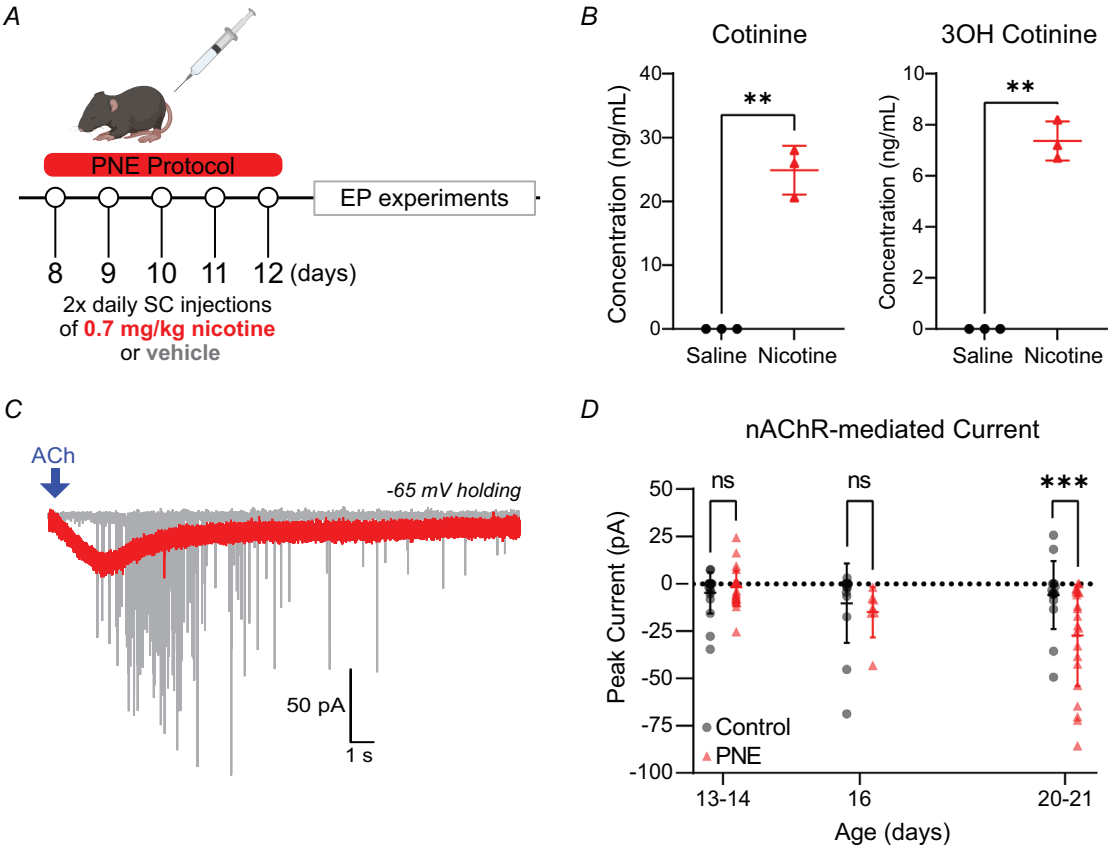

Figure 4. PNE (perinatal nicotine exposure) augments postsynaptic nAChR (nicotinic acetylcholine receptor)-mediated currents in MNTB neurons after hearing onset
A, schematic of nicotine injection protocol used to establish PNE model. *B*, plasma levels of nicotine metabolites 1 h post nicotine or vehicle injection. Cotinine, a major metabolite of nicotine, is significantly increased in the nicotine-injected group 1 h post injection (Welch's t test, P = 0.0078). 3OH cotinine is significantly increased in the nicotine-injected group (Welch's t test, P = 0.0036). *C*, representative trace of nAChR-mediated currents after ACh application in control (grey) and PNE (red) neurons at p20. *D*, quantification of ACh-evoked currents in postsynaptic MNTB neurons across ages in control and PNE animals. There is a significant effect of treatment on current amplitudes, and this effect is most pronounced at the p20–p21 timepoint in PNE mice (two-way ANOVA, P = 0.038, n = 7–35 cells per timepoint per group; Sidak's multiple comparisons at p20–p21: P = 0.001, n = 15–22 cells). [Colour figure can be viewed at wileyonlinelibrary.com]

chamber (A.M. Bickford Inc., Wales Centre, NY, USA). Adult male and female mice aged p20–p24 were utilized for this study. Mice were initially anaesthetized with 3.5% isoflurane and then maintained at 2.5% isoflurane (1 l/min O_2 flow rate) during recordings. Body temperature was maintained at ∼37°C using an electric heating pad on the underside of the mouse. All acoustic stimuli were produced by an auditory evoked potentials workstation (Tucker-Davis Technologies (TDT), Alachua, FL, USA).

Auditory brainstem response test. Subdermal needle electrodes (Rochester Electro-Medical, Lutz, FL, USA) were placed on the top of the head between the ears (active), ipsilateral mastoid (reference) and contralateral mastoid (ground) while the animal was in prone position. Closed-field click stimulus was delivered to the left ear through a 10 cm plastic tube (Tygon, 3.2 mm outer diameter) from a Multi-Field Magnetic Speaker (TDT) at a repeat rate of 16/s. Sound intensities ranged from 90 to 20 dB, with 5 dB decrements. All analyses were performed at 80 dB intensity. Auditory brainstem response (ABR) wave amplitudes were analysed from trough to peak.

Distortion product otoacoustic emission test. Distortion product otoacoustic emission (DPOAE) tests were performed similar to recent work from our laboratory (Nip et al., 2022). Acoustic sound stimuli were delivered through two Multi-Field Magnetic Speakers in 10 cm coupling tubes (TDT) and connected with an ER-10B+ microphone with an ear tip (Etymotic Research, Elk Grove Village, IL, USA) that was inserted into the mouse's left ear canal. Pure tones were presented at 20% frequency

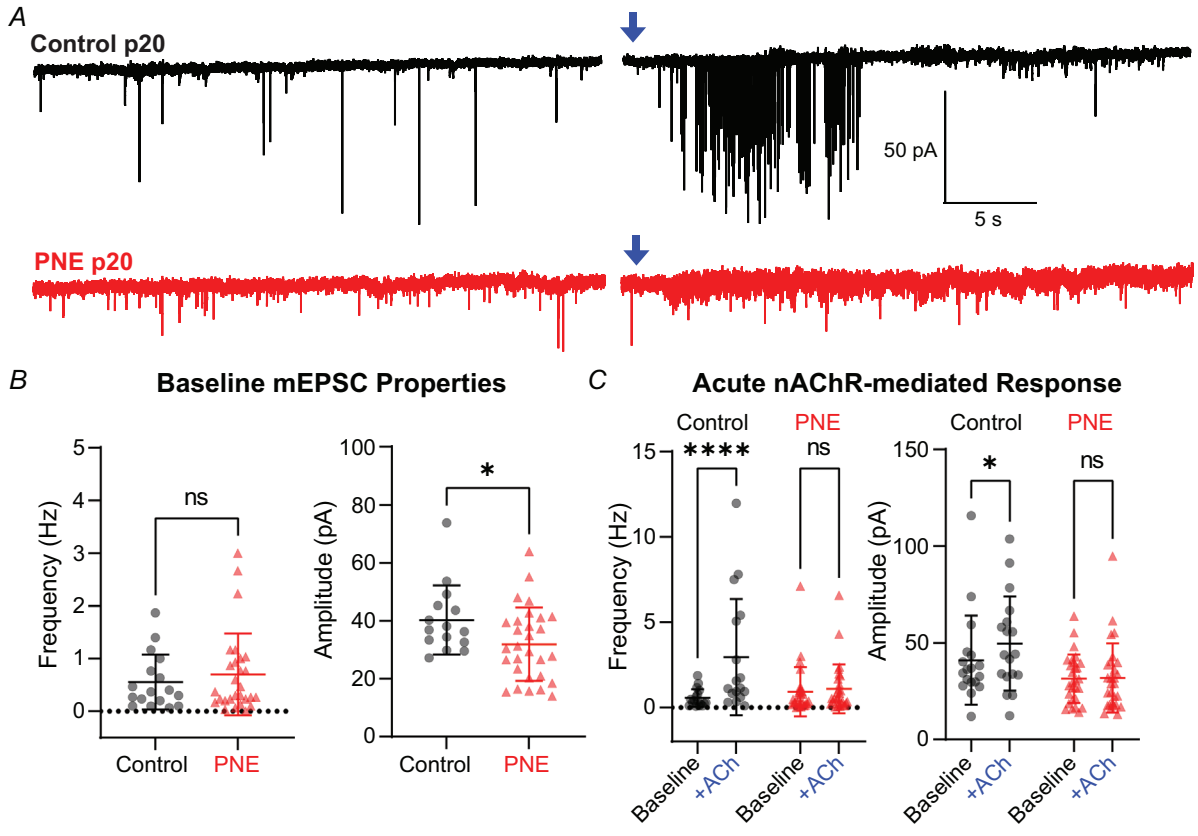

Figure 5. PNE (perinatal nicotine exposure) alters glutamate release and nAChR (nicotinic acetylcholine receptor)-mediated enhancement in the calyx terminal
A, representative traces of mEPSCs from control (black) and PNE mice (red) at p20. Blue arrows indicate the time of acute ACh application (1 mM, 1 s). *B*, quantitative analysis of baseline mEPSC properties from the 30 s preceding ACh puff. There is no significant change in baseline mEPSC frequency between control and PNE mice (Mann–Whitney *U* test, $P = 0.81$, $n = 17$–28 per group). However, a significant decrease in average baseline mEPSC amplitude is evident in PNE mice (Welch's *t* test, $P = 0.039$, $n = 15$–29 per group). *C*, acute effects on mEPSCs after ACh application in control (black) and PNE mice (red). Like control animals in Fig. 2 vehicle control mice had increased mEPSC frequency and amplitude in response to ACh (Fisher's LSD (least significant difference) test, $P < 0.0001$ and $P = 0.042$, respectively, $n = 17$–18 cells). In PNE mice, ACh puff had no significant impact on mEPSC frequency (Fisher's LSD test, $P = 0.67$, $n = 28$ cells) or mEPSC amplitude (Fisher's LSD test, $P = 0.88$, $n = 28$ cells). [Colour figure can be viewed at wileyonlinelibrary.com]

separation between f1 and f2 at 4, 8, 12, 16 and 32 kHz, with intensities starting from 80 to 20 dB, decreasing by 10 dB at each presentation. A total of 512 sweeps were averaged by the RZ6 processor (TDT), and distortion products were calculated as the noise floor subtracted from 2f1-f2.

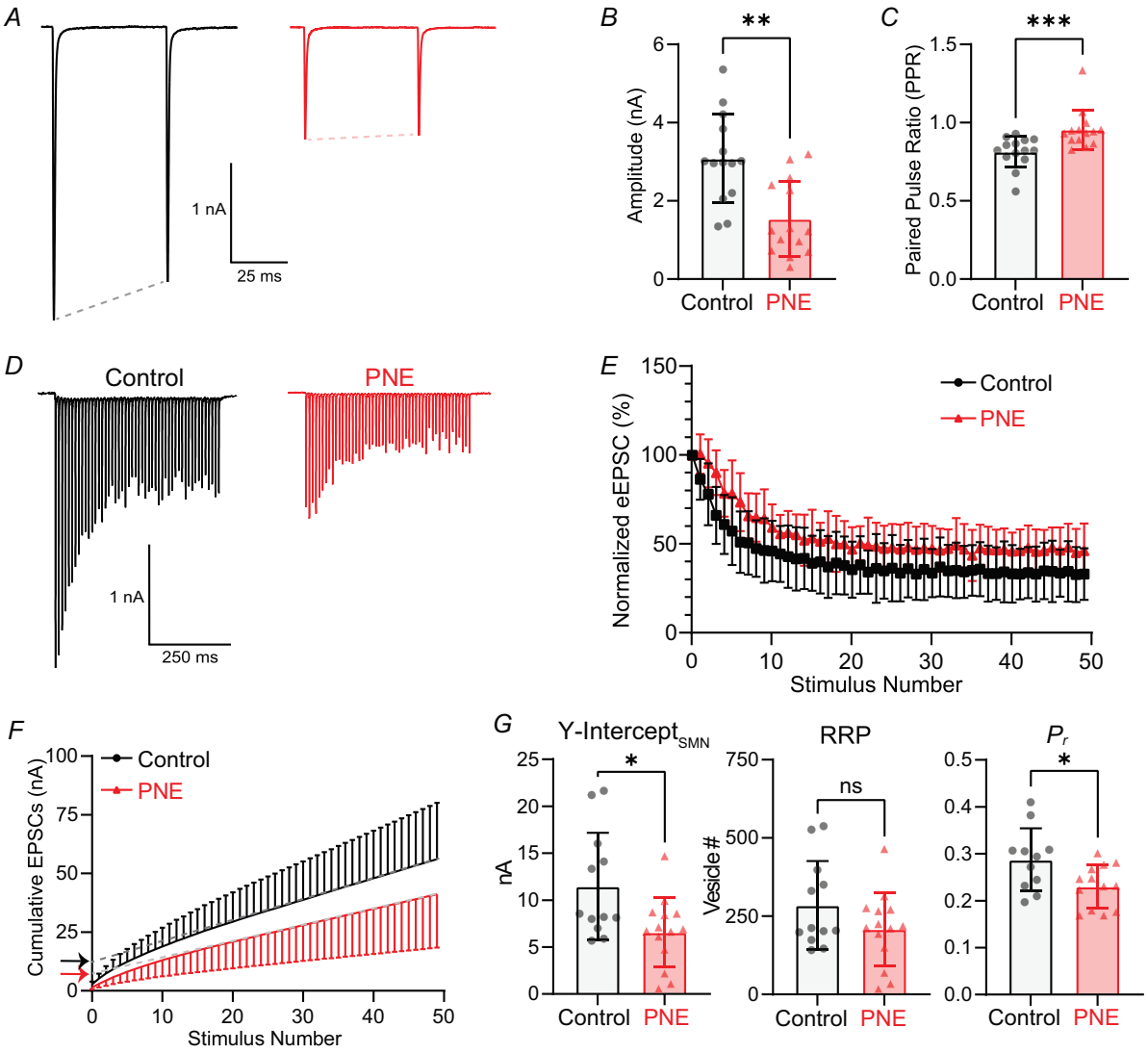

Figure 6. PNE (perinatal nicotine exposure) impairs glutamatergic neurotransmission at the calyx-MNTB synapse
A, representative traces of evoked paired EPSCs (miniature EPSCs, 50 ms interstimulus interval) from control (black) and PNE (red) in response to afferent fibre stimulation. *B*, the amplitude of the first EPSC is significantly reduced in PNE mice (Mann–Whitney *U* test, $P = 0.001$, $n = 14$ cells/group). *C*, paired-pulse ratio (PPR) is quantified from EPSC2/EPSC1. PPR is higher in PNE mice compared to control (Mann–Whitney *U* test, $P = 0.0002$, $n = 14$ cells/group). *D*, representative traces of a 100 Hz train stimulation (500 ms) from control and PNE. *E*, EPSC amplitudes normalized to first EPSC during 100 Hz train, with significantly less depression observed in PNE mice compared to control (two-way ANOVA, $P = 0.014$, $n = 13$–14 cells/group). *F*, cumulative EPSC amplitudes are plotted across the 50 stimulations in the 100 Hz train. *Y*-intercepts (indicated by arrows) are estimates from linear regression back-extrapolated using the steady-state portion of the cumulative EPSC graph (last 10 points) to yield values proportional to RRP (readily releasable pool) size. *G*, the *Y*-intercept is significantly reduced in PNE mice (Welch's *t* test, $P = 0.019$, $n = 12$–14 cells/group). The RRP, calculated from the *Y*-intercept/mEPSC amplitudes, shows no significant difference in vesicle number between groups (Welch's *t* test, $P = 0.15$, $n = 12$–14 cells/group). Probability of release (P_r) is determined by dividing the first EPSC amplitude by the cumulative EPSC amplitude, revealing a significant decrease in P_r in PNE mice compared to control (Welch's *t* test, $P = 0.028$, $n = 11$–13 cells/group). [Colour figure can be viewed at wileyonlinelibrary.com]

Statistical analysis

All statistical analyses were performed in GraphPad Prism, version 9.2.0, for Windows (GraphPad Software, San Diego, CA, USA). The normality of the datasets was analysed using the Kolmogorov–Smirnov test. Parametric or non-parametric tests were carried out accordingly. To compare the two groups an unpaired *t* test using Welch's correction (parametric) or Mann–Whitney *U* test (non-parametric) was carried out. For mEPSC analysis comparing frequency and amplitude before and after ACh application, paired *t* tests or Wilcoxon matched pairs tests were used. To compare current amplitudes across ages, one-way or two-way ANOVA was used. Figures represent data as mean ± SD in figures and results. Linear regressions shown in Fig. 1 utilize *t* tests to test if slopes are significantly non-zero.

Results

Functional expression of nAChRs at the calyx-MNTB synapse during postnatal development

We investigated the expression of nAChRs and their activity at the calyx-MNTB synapse during postnatal development. Previous work has demonstrated the expression of $\alpha7$ nAChRs within the MNTB peaks during the second postnatal week via *in situ* hybridization (Happe & Morley, 2004). To assess the functional expression of nAChRs, we conducted whole-cell patch-clamp recordings to measure ACh-evoked currents and membrane potential changes in MNTB principal neurons across postnatal development (from p8 to p20). In presence of atropine (1 μM) in the bath solution to block muscarinic effects, local application of acetylcholine (ACh, 1 mM) with short pressure puff (1 s) on the MNTB neuron induced ACh-evoked currents in voltage clamp mode (holding at −65 mV). The average amplitude of ACh-evoked currents was −32.8 ± 7.48 pA ($n = 6$ cells) at p8, which significantly reduced to an average amplitude of −2.8 ± 10.99 pA ($n = 6$ cells) by p20 (Fig. 1*A-B*; one-way ANOVA, $P = 0.000189$, $n = 6$–18 cells/timepoint). Plotting of the amplitude against postnatal age was fit by linear regression illustrating a significantly non-zero slope (slope = 1.854, $R^2 = 0.480$, *t* test, $F = 7.386$, $P = 0.0263$). Our results revealed a significant decline in ACh-evoked inward currents in MNTB principal neurons during postnatal development.

In addition to measuring ACh-evoked currents, we evaluated age-dependent changes in membrane potential in response to ACh puff. At p9 ACh puff application caused a consistent and clear depolarization of the membrane potential in MNTB neurons by +2.4 ± 2.66 mV ($n = 12$ cells). However, this depolarization was not sufficient to evoke action potentials in MNTB neurons. Like ACh-evoked currents, this ACh-evoked depolarization diminished over development and eventually resulted in hyperpolarization by p18 (−1.53 ± 4.97 mV, $n = 6$ cells). The statistical analysis revealed a significant change in ACh-evoked membrane potential change across postnatal development (Fig. 1*C-D*; one-way ANOVA, $P = 0.00286$, 6–29 cells/timepoint). A linear regression analysis revealed a significant non-zero slope when fitting membrane potential changes against postnatal age, indicating an age-dependent decline in functional nAChRs (*t* test, $F = 21.8$, $P = 0.00550$). Taken together, the results highlight the developmental changes in functional nAChR expression in postsynaptic MNTB neurons.

Previous work has demonstrated the involvement of $\alpha4\beta2$ and $\alpha7$ nAChRs in the activity of MNTB neurons *in vivo* (Zhang et al., 2021). To determine the specific nAChR subtypes mediating ACh-evoked currents in MNTB neurons, we employed selective antagonists, DHβE and MLA, for $\alpha4\beta2$ and $\alpha7$ nAChRs, respectively. We recorded ACh-evoked currents in MNTB neurons from mice aged p9–p10 to maximize current amplitudes. Our experimental design was as follows: one ACh puff application at 0 min followed by either bath application of control ACSF or ACSF containing a selective nAChR antagonist at 4 min and then a second ACh puff at 9 min. In control aCSF, repeated application of ACh (1 mM) at 9-min intervals led to a decrease in the amplitude of ACh-evoked currents due to receptor desensitization (Fig. 2*A, D*; paired *t* test: −15.65 ± 16.37 to −11.85 ± 14.12 pA, $n = 11$ cells, $P = 0.00428$). Desensitization of nAChRs in response to repeated agonist application is well documented (Giniatullin et al., 2005; Paradiso & Steinbach, 2003); thus, even in the absence of nAChR antagonists, ACh-evoked currents decrease in amplitude with subsequent ACh applications. To account for desensitization, we calculated the 'paired-puff ratio', current amplitude from second puff/current amplitude from first puff, and compared it between control ACSF and selective nAChR antagonist treatments. A significantly smaller paired-puff ratio in presence of an antagonist indicates the involvement of the antagonized nAChR subtype in mediating ACh-evoked currents. Our results revealed an average paired-puff ratio of 0.71 ± 0.23 in the control ACSF condition. There was a significant effect of drug treatment on the paired-puff ratio across all treatments (one-way ANOVA, $P = 0.00927$, $F = 5.777$). The paired-puff ratio is not significantly different between control and MLA treatments (Fig. 2*E*; Dunnett's multiple comparisons test, MLA: 0.71 ± 0.34, $P = 0.999$, $n = 11$ and 8). However, the paired-puff ratio is significantly smaller than control in DHβE condition (control: 0.71 ± 0.23, DHβE: 0.26 ± 0.33, $P = 0.0136$, $n = 11$ and 7). These data suggest that DHβE-sensitive receptors ($\alpha4\beta2$ nAChRs) contribute significantly to the

postsynaptic currents observed in pre-hearing MNTB neurons.

The activation of nAChR enhances vesicular glutamate release from the calyx terminal

Upon postsynaptic recording from mice after p14 when postsynaptic ACh-evoked currents were almost diminished, we found an increase in spontaneous excitatory postsynaptic currents (sEPSCs) after ACh application. To investigate the presence of nAChR at the presynaptic terminals and the impact of its activation on presynaptic vesicular glutamate release, we recorded mEPSCs in MNTB neurons from hearing mice (p14–p22). To avoid the effect of ACh-evoked muscarinic receptor activation at the presynaptic terminal, we used atropine (1 μM) for all mEPSC experiments. In presence of TTX (0.5 μM) and atropine (1 μM), we recorded mEPSCs from MNTB principal neurons before and after ACh puff. Compared to baseline, the frequency and amplitude of mEPSCs significantly increased after ACh application (Fig. 3*A*–*B*; Wilcoxon matched pairs test of frequency: 0.8177 ± 0.27 to 3.455 ± 0.67 Hz, $P < 0.0001$, $n = 32$ cells; amplitude: 43.22 ± 4.16 to 52.85 ± 4.98 pA, $P = 0.0069$, $n = 33$ cells). This indicates that presynaptic nAChR activation increases spontaneous vesicular glutamate release from the calyx terminal. Furthermore, the quantitative analysis of mEPSC amplitude using a cumulative frequency graph and a frequency distribution histogram, showing the rightward shift of mEPSC amplitude distribution after ACh application, supports the increase in glutamatergic transmission at the calyx of Held synapse (Fig. 3*C*). We also recorded ACh-induced currents directly from voltage-clamped calyx terminals where we measured small but significant current amplitudes in four of five cells. Of calyces with an observable current amplitude, the average amplitude was −4.895 ± 4.248 pA (data not shown). To examine if the effect of nAChR activation on glutamate release was dependent on calcium influx into the presynaptic terminal, we performed the same experiments in a calcium-free extracellular condition using ACSF where $CaCl_2$ was replaced with $MgCl_2$ (0 mM $CaCl_2$ and 3 mM $MgCl_2$). In the absence of extracellular calcium, nAChR activation by ACh puff had no effect on mEPSC frequency and amplitude (Fig. 3*D*-*E*; frequency: $P = 0.16$, $n = 11$ cells; amplitude: $P = 0.69$ using Wilcoxon matched pairs test, $n = 10$ cells), indicating calcium flux is important for nAChR activation-mediated glutamate release at the calyx terminal. We examined if ACh-evoked effects on mEPSCs are mediated by α7 nAChRs, which has a high calcium permeability relative to other nAChR subtypes. We measured mEPSC frequency and amplitude in response to ACh in presence of MLA, a selective α7 nAChR antagonist. With α7 nAChRs antagonized, ACh puff had no effect on mEPSC frequency or amplitude (Fig. 3*F*-*G*; frequency: $P = 0.71$, $n = 13$ cells; amplitude: $P = 0.79$, $n = 12$ cells using paired *t* tests). The results suggest that after hearing onset, presynaptic α7 nAChR activation enhances vesicular glutamate release at the calyx terminal that is dependent on calcium flux into the presynaptic terminal.

PNE increases nAChR-mediated currents in postsynaptic MNTB neurons after hearing onset

Chronic nicotine exposure has been known to upregulate nAChR expression across brain regions (Fenster et al., 1999; Hsieh et al., 2002; Vallejo, 2005). To investigate the impact of developmental nicotine exposure on nAChR functional expression at pre- and postsynaptic terminals and synaptic function in the MNTB during the early stages of postnatal development, we established a PNE mouse model. In our PNE protocol, nicotine (0.7 mg/kg free base) or saline vehicle was administered to mouse pups (p8–p12, before hearing onset) twice daily via subcutaneous injections (Fig. 4*A*). We measured nicotine and its metabolites in the plasma of our animals 1 h after injection and found significantly elevated levels of COT and 3OH COT in the nicotine-injected group (Fig. 4*B*). Using PNE mice, we evaluated the effects of nicotine exposure on postsynaptic nAChR-mediated currents during postnatal development. Notably, PNE mice exhibited larger postsynaptic ACh-evoked currents after hearing onset compared to vehicle-treated mice. This effect was most pronounced at p20–p21 (Fig. 4*C*-*D*, two-way ANOVA: $P = 0.038$, $n = 7$–35 cells per timepoint; Sidak's multiple comparisons between control and PNE at p20–p21: $P = 0.001$, $n = 15$–22 cells). PNE before hearing onset (p8–p12) induced a sustained increase in ACh-evoked currents in MNTB neurons, which persists through hearing ages. This result suggests that nicotine exposure has a significant impact on the developmental patterning of nAChR expression in postsynaptic MNTB neurons in the auditory brainstem.

PNE modifies presynaptic nAChR expression and its influence on glutamate release at the calyx terminal

In control mice, nAChR activation by ACh puff enhances the spontaneous release of vesicular glutamate at the presynaptic terminal after hearing onset (Fig. 3). Next, we investigated whether PNE impacts nAChR-mediated presynaptic glutamate release. mEPSC frequency and amplitude were analysed in control and PNE mice (at p20) before (baseline) and after ACh application. At baseline, there was no significant difference in the frequency of mEPSCs between PNE and control mice (control: 0.55 ± 0.13 Hz *vs.* PNE: 0.70 ± 0.15 Hz, Mann–Whitney *U* test, $P = 0.81$, $n = 17$–28 cells/group). However, the

amplitude of mEPSC was significantly decreased in PNE mice compared to control (control: 40.28 ± 3.07 pA *vs*. PNE: 31.92 ± 2.35 pA, Welch's *t* test, $P = 0.039$, $n =$ 15–29 cells/group), suggesting an impairment in synaptic transmission in PNE mice (Fig. 5*A*-*B*). In response to an ACh puff, control mice exhibited a significant increase in both mEPSC frequency and amplitude (Fig. 5*C*, Fisher's least significant difference (LSD) test, $P < 0.0001$ and $P = 0.042$, $n = 17$ and 18 cells, respectively), whereas PNE mice exhibited no significant change in either mEPSC frequency (Fisher's LSD test, $P = 0.67$, $n = 28$ cells) or amplitude (Fisher's LSD test, $P = 0.88$, $n = 28$ cells) after acute ACh application. The results indicate that PNE disrupts the functional role of nAChR in the regulation of neurotransmitter release at the presynaptic terminal. Furthermore, PNE led to a reduction in baseline mEPSC amplitude in PNE mice, indicating the detrimental effects of PNE on synapse development. Overall, these findings suggest that PNE diminishes presynaptic nAChR expression and impairs synaptic transmission at the calyx-MNTB synapse.

PNE impairs glutamatergic neurotransmission at the calyx-MNTB synapse

PNE alters baseline mEPSC properties in the absence of acute ACh application (Fig. 5). To investigate the impact of PNE on glutamatergic neurotransmission at the calyx-MNTB synapse, we recorded eEPSC in MNTB principal neurons using afferent fibre stimulation. We used strychnine (2 μM, glycine receptor antagonist) and bicuculline (20 μM, $GABA_A$ receptor antagonist) to avoid the interference of inhibitory synaptic inputs. We found that PNE resulted in a significant decrease in the amplitude of eEPSCs recorded from MNTB principal neurons at p20. The amplitude of eEPSC in PNE mice was significantly decreased compared to control (Fig. 6*A*-*B*, control: 3.08 ± 1.13 nA *vs*. PNE: 1.54 ± 0.96 nA; Mann–Whitney *U* test, $P = 0.00118$, $n = 14$ cells/group). To further evaluate release probability, we utilized a paired-pulse protocol with a 50 ms interstimulus interval and quantified the paired-pulse ratio (PPR), which is the amplitude ratio of the second EPSC to the first EPSC (EPSC2/EPSC1). In PNE mice, PPR is significantly increased compared to control (Fig. 6*C*, 0.96 ± 0.12 and 0.81 ± 0.09, respectively, Mann–Whitney *U* test, $P = 0.000213$, $n = 14$ cells/group). These results indicate that PNE disrupts glutamatergic transmission at the calyx-MNTB synapse by reducing presynaptic release probability and decreasing glutamate-mediated currents.

Furthermore, we analysed the RRP size and P_r using eEPSC trains at 100 Hz stimulation. During a 100 Hz stimulation train, the amplitudes of eEPSCs gradually decreased in both control and PNE mice, referred to as short-term depression. When normalizing subsequent EPSC amplitudes to the first EPSC, we found significantly less depression in PNE compared to control (Fig. 6*D*-*E*, Two-way ANOVA, $P = 0.0139$, $n =$ 13–14 cells/group). To estimate RRP size and P_r, we used the SMN method (Schneggenburger et al., 1999), which plots cumulative EPSC amplitude against the stimulation number. A linear regression fitted to the steady state (last 10 EPSCs) is back-extrapolated to the *Y*-axis to give a *Y*-intercept value which is proportional to RRP (Fig. 6*F*). The *Y*-intercept values were significantly reduced in PNE mice (control: 11.49 ± 5.69 nA *vs*. PNE: 6.58 ± 3.70 nA, Welch's *t* test, $P = 0.0196$, $n =$ 12–14 cells/group). To estimate RRP size, we divided the *Y*-intercept value by the average group mEPSC amplitude to yield an approximate number of glutamate vesicles per calyx terminal. After this correction was made, we observed no significant difference in RRP between groups (Fig. 6*G*, control: 285.1 ± 141.3 vesicles *vs*. PNE: 208.5 ± 117.3 vesicles, Welch's *t* test, $P = 0.151$, $n =$ 12–14 cells/group). P_r was calculated by dividing the *Y*-intercept value by the first eEPSC amplitude. In PNE mice, P_r of glutamate vesicles at the calyx terminal was significantly lower compared to control (control: 0.29 ± 0.06 *vs*. PNE: 0.23 ± 0.04, Welch's *t* test, $P = 0.0281$, $n =$ 11–13 cells/group). Overall, the results demonstrate that PNE disrupts glutamatergic transmission at the calyx-MNTB synapse by reducing presynaptic release probability and decreasing glutamate-mediated currents.

Effects of PNE on auditory brainstem responses and cochlear function in mice

Next, we investigated the systemic impact of alterations in nAChR expression and synaptic transmission resulting from PNE on *in vivo* auditory function. To gain a comprehensive understanding of the relationship between PNE-induced alterations at the cellular level and the effects on auditory processing, we utilized the ABR test. In response to a sound stimulus, an experimenter will observe five distinct waves of neuronal activity corresponding to (i) auditory nerve, (ii) cochlear nucleus, (iii) SOC, (iv) inferior colliculus and (v) medial geniculate nucleus. We assessed auditory function in both control and PNE animals at p21 by measuring ABRs from each group (Fig. 7*A*, control in black, PNE in red). Specifically we evaluated ABR thresholds, the minimum intensity (dB sound pressure level (SPL)) of a sound stimulus required to elicit five distinguishable ABR peaks from a given animal, and quantified the amplitudes and latencies of peaks from ABR recordings between the two groups. There was a significant increase in ABR click threshold in the PNE group compared to the control group (Fig. 7*B*, Mann–Whitney *U* test, $P = 0.0219$, $n =$ 11–14 mice/group). The elevated ABR threshold indicates that PNE caused a reduction in the sensitivity of the auditory system to sound. To further understand the impact of

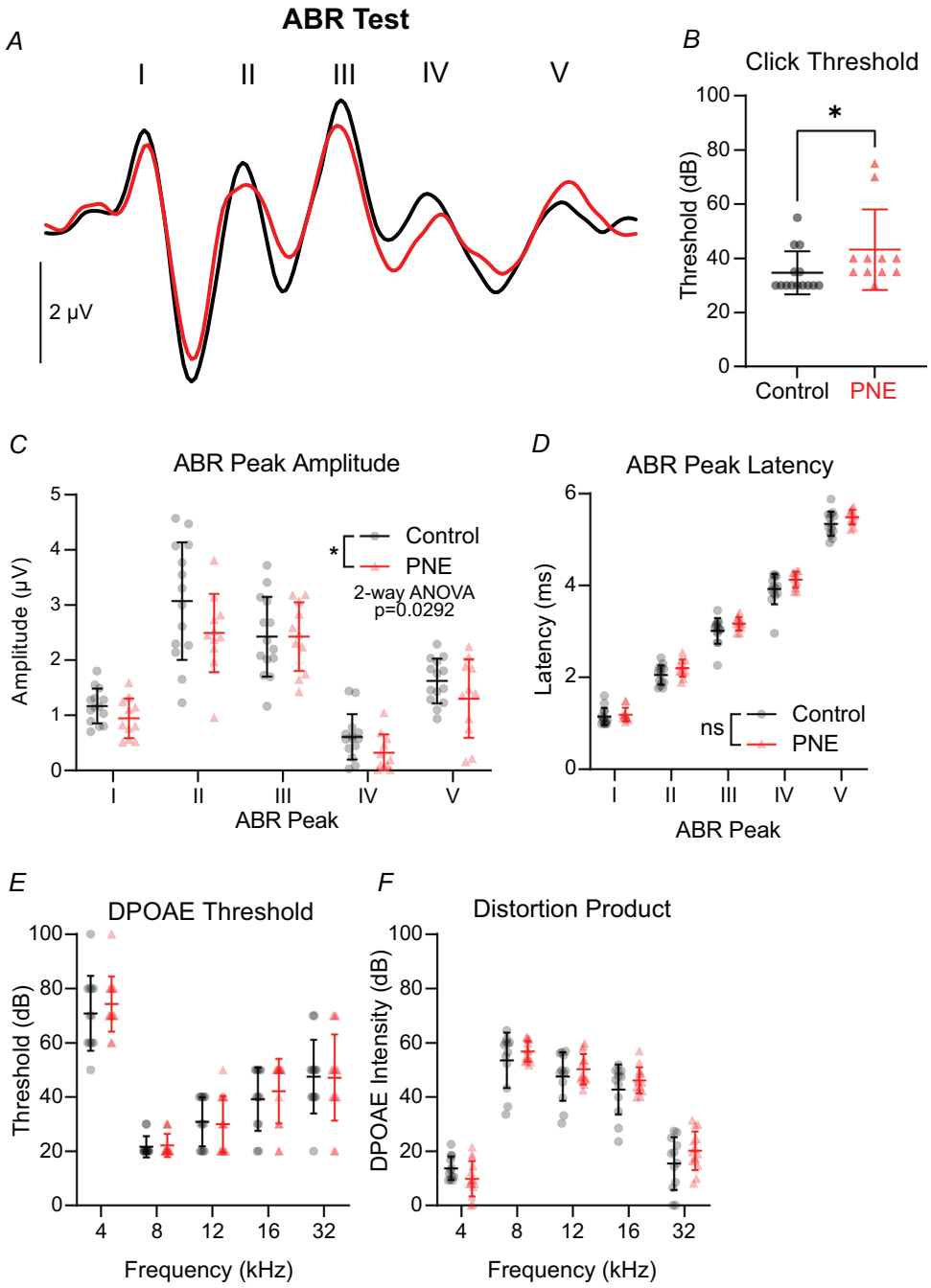

Figure 7. Impact of PNE (perinatal nicotine exposure) on auditory brainstem responses (ABRs) and cochlear function in mice
A, representative ABR traces evoked by click stimuli at 90 dB SPL from control (black) and PNE (red) mice at p21. *B*, a summary of ABR click thresholds in control and PNE mice, demonstrating a significant increase in ABR threshold in PNE mice (Mann–Whitney *U* test, $P = 0.021$, $n = 11$–14 mice/group). *C*, ABR amplitudes measured at 80 dB SPL in control and PNE mice, with PNE inducing a significant reduction in ABR amplitude compared to controls (two-way ANOVA, $P = 0.029$, $n = 11$–14 mice/group). *D*, peak latencies of ABR waves at 80 dB SPL in control and PNE mice, showing no significant effect of treatment on ABR wave peak latencies (two-way ANOVA, $P = 0.07$, $n = 11$–14 mice/group). All bars in graphs represent mean ± SD. *E*, using DPOAE (distortion product otoacoustic emission) test threshold sound intensity required to detect a distortion product was measured across frequencies. PNE did not significantly affect the threshold intensity required to detect a distortion product (DP, two-way ANOVA, $P = 0.60$, $n = 12$–14 mice/group). *F*, DPs generated during the DPOAE test, where PNE does not significantly impact the intensity of DPs (two-way ANOVA, $P = 0.37$, $n = 12$–14 mice/group). [Colour figure can be viewed at wileyonlinelibrary.com]

PNE on auditory processing, we quantified the amplitudes and latencies of each peak in the ABR. Our analysis revealed that at 80 dB, the peak amplitudes of the ABR were significantly lower in PNE compared to control mice using two-way ANOVA (Fig. 7*C*, $P = 0.0292$, $n =$ 11–14 mice/group); however, *post hoc* analyses indicate that no individual peaks are significantly decreased in the PNE animals (Sidak's multiple comparisons test, peak I: $P = 0.473$, peak II: $P = 0.463$, peak III: $P = 0.999$, peak IV: $P = 0.285$, peak V: $P = 0.678$). This result suggests a decrease in sound-evoked neuronal activity in each auditory nucleus in response to a click stimulus. However, there was no effect of treatment on ABR peak latency, indicating no effect on central conduction speed (Fig. 7*D*, two-way ANOVA, $P = 0.0736$, $n =$ 11–14 animals/group). Additionally, we sought to determine whether the observed changes in ABRs were only due to central processing deficits or if the peripheral auditory system was also affected by PNE. To assess outer hair cell function in the cochlea, we used the DPOAE test. Like ABR measurements we determined DPOAE thresholds, the minimum intensity of a sound stimulus required to elicit a detectable distortion product, and measured distortion product, the intensity (dB SPL) of the amplification product elicited by outer hair cells in response to the sound stimulus. There was no significant difference in distortion product threshold between control and PNE mice (Fig. 7*E*, two-way ANOVA, $P = 0.602$, $n =$ 12–14 mice/group) nor distortion product intensity (Fig. 7*F*, two-way ANOVA, $P = 0.378$), indicating no significant impact of PNE on cochlea function. These results suggest that the observed ABR phenotypes were likely due to central processing deficits rather than peripheral auditory dysfunction. More specifically, PNE has significant impacts on the auditory brainstem rather than the peripheral system. Taken together, our results provide evidence that PNE can induce significant changes in auditory function at the cellular level, ultimately impacting auditory development.

Discussion

Our study uncovers the adverse effects of PNE on the glutamatergic synaptic mechanisms and auditory processing in juvenile mice, highlighting the critical alterations in nAChR function within the MNTB. We found a diminished functional expression of postsynaptic nAChRs during the early postnatal period, whereas presynaptic nAChR activity, which is key for glutamate release, becomes more prominent after the onset of hearing. PNE disrupts this developmentally regulated pattern of nAChR expression, leading to impaired synaptic transmission at the calyx of Held-MNTB synapse. Additionally, PNE mice exhibit increased ABR thresholds and reduced peak amplitudes, indicating impaired central auditory processing without cochlear function changes.

Diversity of nAChR expression and function in the CNS

Previous studies indicate that nAChR subunit expression patterns vary across brain regions during postnatal development, with distinct developmental patterns observed in the brainstem, cerebellum and striatum (Azam et al., 2007; Shacka & Robinson, 1998; Son & Winzer-Serhan, 2006; Zhang et al., 1998). For example, $\alpha 7$ subunit mRNAs exhibit consistent expression in the brainstem but a bell-shaped developmental pattern in the striatum. In the auditory system, nAChR expression is initially widespread in the cochlear nucleus and SOC but becomes more restricted to specific cell types and synaptic compartments during development (Happe & Morley, 2004; Zhang et al., 2021). Our study revealed that nAChRs are expressed in both pre- and postsynaptic compartments of the MNTB synapse with discrete developmental patterning. It is possible that pre- and postsynaptic nAChRs have different expression timing due to differences in subunit composition (Azam et al., 2007; Zhang et al., 1998).

Functional differences in nAChR subunit composition allow for discrete pharmacological and physiological characteristics. Our data demonstrated that $\alpha 4\beta 2$ nAChRs are responsible for a significant portion of nAChR currents from postsynaptic MNTB neurons. $\alpha 4\beta 2$ nAChRs are the most prevalent nAChR subunit conformation in the brain, which exhibit slow channel kinetics, low calcium permeability and soma/postsynaptic density localization (Posadas et al., 2013). Due to their high affinity for nicotine, $\beta 2$-containing nAChRs are required for mediating the reinforcing effects of nicotine (Epping-Jordan et al., 1999; Picciotto et al., 1998). The developmental role of $\alpha 4\beta 2$ nAChRs is less well characterized, but maturation and patterning of retinothalamic projections require periodic waves of action potentials that are dependent on $\beta 2$-containing nAChRs (Feller et al., 1996; Penn et al., 1998). The role of $\alpha 4\beta 2$ nAChRs in MNTB neuron development has yet to be explored. Due to their diverse functional profiles, MNTB principal neurons may express specific nAChR subtypes to stabilize calyx-MNTB synapse formation and subsequently downregulate or transition to another subunit composition once synapses are structurally mature around p14 (Kandler & Friauf, 1993).

In the adult brain, presynaptic nAChR localization is prevalent at glutamatergic synapses, such as terminals in the ventral tegmental area and hippocampus (Fabian-Fine et al., 2001; Jones & Wonnacott, 2004). Although we cannot definitively conclude the role of presynaptic nAChRs in neurotransmitter release at the calyx terminal,

we hypothesize they respond to top-down cholinergic inputs from the pontomesencephalic tegmentum (PMT) or collaterals from SOC neurons to modulate MNTB activity (Zhang et al., 2021). Our data show that α7 nAChR activation regulates vesicular glutamate release from the calyx terminal in hearing animals. α7 nAChRs typically have fast channel kinetics, high calcium permeability and presynaptic localization, making them well suited for modulating vesicular release (Dani, 2015; Mansvelder & McGehee, 2002). Our data demonstrate an increase in mEPSC frequency and amplitude after ACh puff application in MNTB neurons. One plausible explanation for the observed increase in quantal size is the emergence of multivesicular release from the calyx terminal. Multivesicular structures have previously been visualized in the rat calyx of Held (de Lange et al., 2003). Additionally, a calcium-dependent increase in quantal size at the calyx was reported after high-frequency stimulation, attributed to compound vesicle fusion and subsequent exocytosis (He et al., 2009). In our experiments, it is likely that calcium influx triggered by nAChR activation initiates a similar mechanism at the calyx terminal, resulting in the observed increase in quantal size. Taken together, with our findings cholinergic inputs to the MNTB enhance vesicular glutamate release from the calyx via α7 nAChRs to modulate synaptic transmission after hearing onset.

Effect of PNE on nAChR patterning and glutamatergic neurotransmission

PNE has been shown to impair the maturation of glutamatergic neurotransmission in the brainstem in globular cells of the VNLL (Baumann & Koch, 2017). Our study found that PNE caused a significant decrease in functional presynaptic nAChRs at the calyx terminal but interestingly a significant increase in postsynaptic nAChR-evoked currents in MNTB neurons at p20–p21. An increase in functional postsynaptic nAChRs in the PNE is supported by the observed increased nAChR expression across human and animal models alike in response to chronic nicotine exposure (Breese et al., 1997; Harkness & Millar, 2002; Perry et al., 1999; Vallejo, 2005). Our results showed that PNE disrupted or delayed developmental changes in nAChR expression at pre- and postsynaptic compartments, which could have lasting effects on glutamate signalling and brain development. It remains to be determined whether this postsynaptic effect persists into adulthood or if the increase in nAChR-mediated currents is transient.

Impaired glutamatergic signalling after PNE is demonstrated by reduced mEPSC and eEPSC amplitudes but no change in RRP size, suggesting decreases in quantal size but no change in quantal content (Fig. 6). It is possible that the impaired calyx-MNTB neurotransmission is a secondary effect of disrupted nAChR patterning. PNE has been shown to alter the expression and function of nAChRs across brain regions, leading to changes in presynaptic release and glutamatergic neurotransmission (Abdulla et al., 1996; Parameshwaran et al., 2012; Pilarski et al., 2012; Proctor et al., 2011). Genetic deletion of α7 nAChRs decreases mEPSC frequency in cortical and hippocampal neurons, indicating reduced number of glutamatergic synapses (Lozada et al., 2012; Zhong et al., 2022). Additionally, PNE could impact presynaptic glutamate release through alterations in calcium signalling in the hippocampus and cortex (Hayashida et al., 2005; Katsura & Ohkuma, 2005; Katsura et al., 2002). Acute nAChR activation increases spontaneous glutamate vesicle fusion (Le Magueresse et al., 2006; Proctor et al., 2011; Puddifoot et al., 2015; Sharma & Vijayaraghavan, 2003; Tang et al., 2015; Zhong et al., 2008) and specifically increases release probability demonstrated by decreased PPR in hippocampal neurons (Cheng & Yakel, 2014; Damborsky et al., 2015; Sola et al., 2006). Our study showed acute ACh application increased glutamate release and prolonged nAChR activation in PNE mice reduced release probability (Figs 3 and 6). Therefore, if PNE decreases presynaptic nAChR expression or its activity, this could contribute to decreased release probability of vesicular glutamate observed at the calyx terminal.

Moreover, PNE could modulate synaptic transmission by decreasing α-amino-3-hydroxy-5-methyl-4-isoxazolepropionic acid receptor (AMPAR) expression in the postsynaptic membrane. Genetic deletion of neuroligin 3, a protein key for AMPAR stabilization in the postsynaptic membrane, has been shown to decrease eEPSC amplitude at the calyx terminal, similar to our PNE model (Han et al., 2022). PNE-induced decrease in mEPSC and eEPSC amplitude might be driven by both postsynaptic changes (e.g. a decrease in AMPAR expression, density or clustering) and presynaptic mechanisms. Previous work observed a reduction in VGLUT1 and PSD95 in hippocampal synaptosomes after prenatal nicotine exposure (Parameshwaran et al., 2012). PNE has been shown to alter both presynaptic release mechanisms and postsynaptic receptor expression, leading to long-lasting changes in glutamate signalling and subsequent effects on brain development and function.

Physiological relevance

PNE-induced impairment of glutamatergic neurotransmission and altered nAChR expression in the MNTB might have important physiological consequences for auditory processing. The calyx of Held-MNTB synapse is critical for precise encoding of sound onset time, and

intensity, and sound localization (Beiderbeck et al., 2018; Englitz et al., 2009; Guinan & Li, 1990). Our data reveal that PNE mice exhibit an elevated click ABR threshold and decreased ABR peak amplitudes, indicating a deficit in central auditory processing. The observed cellular phenotypes impact sound-evoked neuronal population activity via ABR, impairing crucial auditory functions. Additionally, alterations in presynaptic release probability and RRP size could have implications for short-term plasticity, which is thought to play a role in processing complex sounds such as speech (Keine et al., 2022; Singh et al., 2018).

The disruptions in glutamatergic signalling and nAChR expression after PNE could have broader implications for central auditory function, given the widespread distribution of glutamatergic synapses in the auditory brainstem pathway (Petralia & Wenthold, 2009). Disruptions in nAChR signalling have been linked to impaired auditory processing in various conditions, such as schizophrenia-related auditory sensory gating deficits, which can be improved with nAChR agonists (Aidelbaum et al., 2018). Similarly, genetic deletion of α9 nAChR in mice leads to impairment in sound localization and frequency discrimination (Clause et al., 2017). On the contrary, artificially augmenting nAChR signalling to enhance medial olivocochlear efferent activity impairs glutamatergic neurotransmission at the calyx-MNTB synapse and eliminates tonotopic patterning of intrinsic properties of MNTB neurons (di Guilmi et al., 2019). Interestingly, our previous work has observed elimination of MNTB tonotopic gradients in mice with global brain-derived neurotrophic factor (BDNF) reduction (Wollet & Kim, 2022), and neonatal exposure to nicotine reduces brain BDNF levels (Xiaoyu, 2015). Therefore, it is possible that reduction in BDNF after nicotine exposure contributes to the PNE-induced synaptic impairments. In summary, our findings provide novel insights into the underlying mechanisms of auditory deficits after developmental nicotine exposure and emphasize the importance of addressing maternal nicotine intake during pregnancy to mitigate the risk of auditory processing deficits in children.

References

Abdulla, F. A., Gray, J. A., Sinden, J. D., Bradbury, E., Calaminici, M.-R., Lippiello, P. M., & Wonnacott, S. (1996). Relationship between up-regulation of nicotine binding sites in rat brain and delayed cognitive enhancement observed after chronic or acute nicotinic receptor stimulation. *Psychopharmacology*, **124**(4), 323–331.

Aidelbaum, R., Labelle, A., Baddeley, A., & Knott, V. (2018). Assessing the acute effects of CDP-choline on sensory gating in schizophrenia: A pilot study. *Journal of Psychopharmacology*, **32**(5), 541–551.

Aramakis, V. B., Hsieh, C. Y., Leslie, F. M., & Metherate, R. (2000). A critical period for nicotine-induced disruption of synaptic development in rat auditory cortex. *Journal of Neuroscience*, **20**(16), 6106–6116.

Aramakis, V. B., & Metherate, R. (1998). Nicotine selectively enhances NMDA receptor-mediated synaptic transmission during postnatal development in sensory neocortex. *Journal of Neuroscience*, **18**(20), 8485–8495.

Azam, L., Chen, Y., & Leslie, F. M. (2007). Developmental regulation of nicotinic acetylcholine receptors within midbrain dopamine neurons. *Neuroscience*, **144**(4), 1347–1360.

Baumann, V. J., & Koch, U. (2017). Perinatal nicotine exposure impairs the maturation of glutamatergic inputs in the auditory brainstem: Nicotine exposure disturbs maturation of synaptic inputs. *The Journal of Physiology*, **595**(11), 3573–3590.

Beebe, N. L., Zhang, C., Burger, R. M., & Schofield, B. R. (2021). Multiple sources of cholinergic input to the superior olivary complex. *Frontiers in Neural Circuits*, **15**, 715369.

Beiderbeck, B., Myoga, M. H., Müller, N. I. C., Callan, A. R., Friauf, E., Grothe, B., & Pecka, M. (2018). Precisely timed inhibition facilitates action potential firing for spatial coding in the auditory brainstem. *Nature Communications*, **9**(1), 1771.

Breese, C. R., Marks, M. J., Logel, J., Adams, C. E., Sullivan, B., Collins, A. C., & Leonard, S. (1997). Effect of smoking history on [3H]nicotine binding in human postmortem brain. *Journal of Pharmacology and Experimental Therapeutics*, **282**(1), 7–13.

Chen, G., & Yan, J. (2007). Cholinergic modulation incorporated with a tone presentation induces frequency-specific threshold decreases in the auditory cortex of the mouse: Cholinergic facilitation for cortical plasticity. *European Journal of Neuroscience*, **25**(6), 1793–1803.

Cheng, Q., & Yakel, J. L. (2014). Presynaptic α7 nicotinic acetylcholine receptors enhance hippocampal mossy Fiber glutamatergic transmission via PKA activation. *Journal of Neuroscience*, **34**(1), 124–133.

Clause, A., Lauer, A. M., & Kandler, K. (2017). Mice lacking the Alpha9 subunit of the nicotinic acetylcholine receptor exhibit deficits in frequency difference limens and sound localization. *Frontiers in Cellular Neuroscience*, **11**, 167.

Crane, L., Goddard, L., & Pring, L. (2009). Sensory processing in adults with autism spectrum disorders. *Autism*, **13**(3), 215–228.

Damborsky, J. C., Griffith, W. H., & Winzer-Serhan, U. H. (2015). Neonatal nicotine exposure increases excitatory synaptic transmission and attenuates nicotine-stimulated GABA release in the adult rat hippocampus. *Neuropharmacology*, **88**, 187–198.

Dani, J. A. (2015). Neuronal nicotinic acetylcholine receptor structure and function and response to nicotine. In *International Review of Neurobiology* (pp. 3–19). Elsevier.

di Guilmi, M. N., Boero, L. E., Castagna, V. C., Rodríguez-Contreras, A., Wedemeyer, C., Gómez-Casati, M. E., & Elgoyhen, A. B. (2019). Strengthening of the efferent olivocochlear system leads to synaptic dysfunction and tonotopy disruption of a central auditory nucleus. *Journal of Neuroscience*, **39**(36), 7037–7048.

Elgoyhen, A. B., Katz, E., & Fuchs, P. A. (2009). The nicotinic receptor of cochlear hair cells: A possible pharmacotherapeutic target? *Biochemical Pharmacology*, **78**(7), 712–719.

Englitz, B., Tolnai, S., Typlt, M., Jost, J., & Rübsamen, R. (2009). Reliability of synaptic transmission at the synapses of held *in vivo* under acoustic stimulation *PLoS ONE*, **4**(10), e7014.

Epping-Jordan, M. P., Picciotto, M. R., Changeux, J.-P., & Pich, E. M. (1999). Assessment of nicotinic acetylcholine receptor subunit contributions to nicotine self-administration in mutant mice. *Psychopharmacology*, **147**(1), 25–26.

Fabian-Fine, R., Skehel, P., Errington, M. L., Davies, H. A., Sher, E., Stewart, M. G., & Fine, A. (2001). Ultrastructural distribution of the α7 nicotinic acetylcholine receptor subunit in rat hippocampus. *Journal of Neuroscience*, **21**(20), 7993–8003.

Feller, M. B., Wellis, D. P., Stellwagen, D., Werblin, F. S., & Shatz, C. J. (1996). Requirement for cholinergic synaptic transmission in the propagation of spontaneous retinal waves. *Science*, **272**(5265), 1182–1187.

Fenster, C. P., Whitworth, T. L., Sheffield, E. B., Quick, M. W., & Lester, R. A. J. (1999). Upregulation of surface $\alpha4\beta2$ nicotinic receptors is initiated by receptor desensitization after chronic exposure to nicotine. *Journal of Neuroscience*, **19**(12), 4804–4814.

Ghanizadeh, A. (2011). Sensory processing problems in children with ADHD, a systematic review. *Psychiatry Investigation*, **8**(2), 89.

Ghimire, M., Cai, R., Ling, L., Hackett, T. A., & Caspary, D. M. (2020). Nicotinic receptor subunit distribution in auditory cortex: Impact of aging on receptor number and function. *Journal of Neuroscience*, **40**(30), 5724–5739.

Giniatullin, R., Nistri, A., & Yakel, J. (2005). Desensitization of nicotinic ACh receptors: Shaping cholinergic signaling. *Trends in Neurosciences*, **28**(7), 371–378.

Guinan, J. J., & Li, R. Y.-S. (1990). Signal processing in brainstem auditory neurons which receive giant endings (calyces of Held) in the medial nucleus of the trapezoid body of the cat. *Hearing Research*, **49**(1–3), 321–334.

Han, Y., Cao, R., Qin, L., Chen, L. Y., Tang, A.-H., Südhof, T. C., & Zhang, B. (2022). Neuroligin-3 confines AMPA receptors into nanoclusters, thereby controlling synaptic strength at the calyx of Held synapses. *Science Advances*, **8**(24), eabo4173.

Happe, H. K., & Morley, B. J. (1998). Nicotinic acetylcholine receptors in rat cochlear nucleus: [125I]-?-bungarotoxin receptor autoradiography and in situ hybridization of ?7 nAChR subunit mRNA. *Journal of Comparative Neurology*, **397**(2), 163–180.

Happe, H. K., & Morley, B. J. (2004). Distribution and postnatal development of α7 nicotinic acetylcholine receptors in the rodent lower auditory brainstem. *Developmental Brain Research*, **153**(1), 29–37.

Harkness, P. C., & Millar, N. S. (2002). Changes in conformation and subcellular distribution of $\alpha4\beta2$ nicotinic acetylcholine receptors revealed by chronic nicotine treatment and expression of subunit chimeras. *Journal of Neuroscience*, **22**(23), 10172–10181.

Hayashida, S., Katsura, M., Torigoe, F., Tsujimura, A., & Ohkuma, S. (2005). Increased expression of L-type high voltage-gated calcium channel $\alpha1$ and $\alpha2/\delta$ subunits in mouse brain after chronic nicotine administration. *Molecular Brain Research*, **135**(1–2), 280–284.

He, L., Xue, L., Xu, J., McNeil, B. D., Bai, L., Melicoff, E., Adachi, R., & Wu, L.-G. (2009). Compound vesicle fusion increases quantal size and potentiates synaptic transmission. *Nature*, **459**(7243), 93–97.

Hsieh, C. Y., Leslie, F. M., & Metherate, R. (2002). Nicotine exposure during a postnatal critical period alters NR2A and NR2B mRNA expression in rat auditory forebrain. *Developmental Brain Research*, **133**(1), 19–25.

Jones, I. W., & Wonnacott, S. (2004). Precise localization of α7 nicotinic acetylcholine receptors on glutamatergic axon terminals in the rat ventral tegmental area. *Journal of Neuroscience*, **24**(50), 11244–11252.

Kandler, K., & Friauf, E. (1993). Pre-and postnatal development of efferent connections of the cochlear nucleus in the rat. *Journal of Comparative Neurology*, **328**(2), 161–184.

Katbamna, B., Klutz, N., Pudrith, C., Lavery, J. P., & Ide, C. F. (2013). Prenatal smoke exposure: Effects on infant auditory system and placental gene expression. *Neurotoxicology and Teratology*, **38**, 61–71.

Katsura, M., Mohri, Y., Shuto, K., Hai-Du, Y., Amano, T., Tsujimura, A., Sasa, M., & Ohkuma, S. (2002). Up-regulation of L-type voltage-dependent calcium channels after long term exposure to nicotine in cerebral cortical neurons. *Journal of Biological Chemistry*, **277**(10), 7979–7988.

Katsura, M., & Ohkuma, S. (2005). Functional proteins involved in regulation of intracellular Ca^{2+} for drug development: Chronic nicotine treatment upregulates L-type high voltage-gated calcium channels. *Journal of Pharmacological Sciences*, **97**(3), 344–347.

Keine, C., Al-Yaari, M., Radulovic, T., Thomas, C. I., Valino Ramos, P., Guerrero-Given, D., Ranjan, M., Taschenberger, H., Kamasawa, N., & Young, S. M. (2022). Presynaptic Rac1 controls synaptic strength through the regulation of synaptic vesicle priming. *eLife*, **11**, e81505.

King, E., Campbell, A., Belger, A., & Grewen, K. (2018). Prenatal nicotine exposure disrupts infant neural markers of orienting. *Nicotine & Tobacco Research*, **20**(7), 897–902.

Kramarow, E., & Elgaddal, N. (2023). Current Electronic Cigarette Use in Adults Aged 18 and Over: Untied States, 2021. NCHS data brief, (475), 1–8.

de Lange, R. P. J., de Roos, A. D. G., & Borst, J. G. G. (2003). Two modes of vesicle recycling in the rat calyx of Held. *Journal of Neuroscience*, **23**(31), 10164–10173.

Le Magueresse, C., Safiulina, V., Changeux, J.-P., & Cherubini, E. (2006). Nicotinic modulation of network and synaptic transmission in the immature hippocampus investigated with genetically modified mice: Nicotine and synaptic transmission in the developing hippocampus. *The Journal of Physiology*, **576**(Pt 2), 533–546.

Liang, K., Poytress, B. S., Chen, Y., Leslie, F. M., Weinberger, N. M., & Metherate, R. (2006). Neonatal nicotine exposure impairs nicotinic enhancement of central auditory processing and auditory learning in adult rats. *European Journal of Neuroscience*, **24**(3), 857–866.

Lozada, A. F., Wang, X., Gounko, N. V., Massey, K. A., Duan, J., Liu, Z., & Berg, D. K. (2012). Glutamatergic synapse formation is promoted by 7-containing nicotinic acetylcholine receptors. *Journal of Neuroscience*, **32**(22), 7651–7661.

Mansvelder, H. D., & McGehee, D. S. (2002). Cellular and synaptic mechanisms of nicotine addiction. *Journal of Neurobiology*, **53**(4), 606–617.

Marco, E. J., Hinkley, L. B. N., Hill, S. S., & Nagarajan, S. S. (2011). Sensory processing in autism: A review of neurophysiologic findings. *Pediatric Research*, **69**(5 Part 2), 48R–54R.

Metherate, R., Intskirveli, I., & Kawai, H. D. (2012). Nicotinic filtering of sensory processing in auditory cortex. *Frontiers in Behavioral Neuroscience*, **6**, 44.

Nip, K., Kashiwagura, S., & Kim, J. H. (2022). Loss of β4-spectrin impairs nav channel clustering at the heminode and temporal fidelity of presynaptic spikes in developing auditory brain. *Scientific Reports*, **12**(1), 5854.

Paradiso, K. G., & Steinbach, J. H. (2003). Nicotine is highly effective at producing desensitization of rat $\alpha4\beta2$ neuronal nicotinic receptors. *The Journal of Physiology*, **553**(3), 857–871.

Parameshwaran, K., Buabeid, M. A., Karuppagounder, S. S., Uthayathas, S., Thiruchelvam, K., Shonesy, B., Dityatev, A., Escobar, M. C., Dhanasekaran, M., & Suppiramaniam, V. (2012). Developmental nicotine exposure induced alterations in behavior and glutamate receptor function in hippocampus. *Cellular and Molecular Life Sciences*, **69**(5), 829–841.

Penn, A. A., Riquelme, P. A., Feller, M. B., & Shatz, C. J. (1998). Competition in retinogeniculate patterning driven by spontaneous activity. *Science*, **279**(5359), 2108–2112.

Perry, D. C., Dávila-García, M. I., Stockmeier, C. A., & Kellar, K. J. (1999). Increased nicotinic receptors in brains from smokers: Membrane binding and autoradiography studies. *Journal of Pharmacology and Experimental Therapeutics*, **289**(3), 1545–1552.

Petralia, R. S., & Wenthold, R. J. (2009). Neurotransmitters in the auditory system. In *Encyclopedia of Neuroscience* (pp. 2847–2853). Springer.

Picciotto, M. R., Zoli, M., Rimondini, R., Léna, C., Marubio, L. M., Pich, E. M., Fuxe, K., & Changeux, J.-P. (1998). Acetylcholine receptors containing the $\beta2$ subunit are involved in the reinforcing properties of nicotine. *Nature*, **391**(6663), 173–177.

Pilarski, J. Q., Wakefield, H. E., Fuglevand, A. J., Levine, R. B., & Fregosi, R. F. (2012). Increased nicotinic receptor desensitization in hypoglossal motor neurons following chronic developmental nicotine exposure. *Journal of Neurophysiology*, **107**(1), 257–264.

Posadas, I., Lopez-Hernandez, B., & Cena, V. (2013). Nicotinic receptors in neurodegeneration. *Current Neuropharmacology*, **11**(3), 298–314.

Proctor, W. R., Dobelis, P., Moritz, A. T., & Wu, P. H. (2011). Chronic nicotine treatment differentially modifies acute nicotine and alcohol actions on GABAA and glutamate receptors in hippocampal brain slices: Synaptic interactions between nicotine and alcohol. *British Journal of Pharmacology*, **162**(6), 1351–1363.

Puddifoot, C. A., Wu, M., Sung, R.-J., & Joiner, W. J. (2015). Ly6h regulates trafficking of Alpha7 nicotinic acetylcholine receptors and nicotine-induced potentiation of glutamatergic signaling. *Journal of Neuroscience*, **35**(8), 3420–3430.

Rivera-Perez, L. M., Kwapiszewski, J. T., & Roberts, M. T. (2021). $\alpha3\beta4*$ nicotinic acetylcholine receptors strongly modulate the excitability of VIP neurons in the mouse inferior colliculus. *Frontiers in Neural Circuits*, **15**, 709387.

Rowell, P. P., & Li, M. (2002). Dose-response relationship for nicotine-induced up-regulation of rat brain nicotinic receptors. *Journal of Neurochemistry*, **68**(5), 1982–1989.

Schneggenburger, R., Meyer, A. C., & Neher, E. (1999). Released fraction and total size of a pool of immediately available transmitter quanta at a calyx synapse. *Neuron*, **23**(2), 399–409.

Shacka, J. J., & Robinson, S. E. (1998). Postnatal developmental regulation of neuronal nicotinic receptor subunit $\alpha7$ and multiple $\alpha4$ and $\beta2$ mRNA species in the rat. *Developmental Brain Research*, **109**(1), 67–75.

Sharma, G., & Vijayaraghavan, S. (2003). Modulation of presynaptic store calcium induces release of glutamate and postsynaptic firing. *Neuron*, **38**(6), 929–939.

Singh, M., Miura, P., & Renden, R. (2018). Age-related defects in short-term plasticity are reversed by acetyl-L-carnitine at the mouse calyx of Held. *Neurobiology of Aging*, **67**, 108–119.

Sola, E., Capsoni, S., Rosato-Siri, M., Cattaneo, A., & Cherubini, E. (2006). Failure of nicotine-dependent enhancement of synaptic efficacy at Schaffer-collateral CA1 synapses of AD11 anti-nerve growth factor transgenic mice. *European Journal of Neuroscience*, **24**(5), 1252–1264.

Son, J.-H., & Winzer-Serhan, U. H. (2006). Postnatal expression of $\alpha2$ nicotinic acetylcholine receptor subunit mRNA in developing cortex and hippocampus. *Journal of Chemical Neuroanatomy*, **32**(2–4), 179–190.

Sun, W., Hansen, A., Zhang, L., Lu, J., Stolzberg, D., & Kraus, K. S. (2008). Neonatal nicotine exposure impairs development of auditory temporal processing. *Hearing Research*, **245**(1–2), 58–64.

Tang, B., Luo, D., Yang, J., Xu, X.-Y., Zhu, B.-L., Wang, X.-F., Yan, Z., & Chen, G.-J. (2015). Modulation of AMPA receptor mediated current by nicotinic acetylcholine receptor in layer I neurons of rat prefrontal cortex. *Scientific Reports*, **5**(1), 14099.

Vallejo, Y. F. (2005). Chronic nicotine exposure upregulates nicotinic receptors by a novel mechanism. *Journal of Neuroscience*, **25**(23), 5563–5572.

Weimann, S. R., Zhang, C., & Burger, R. M. (2024). A developmental switch in cholinergic mechanisms of modulation in the medial nucleus of the trapezoid body. *Journal of Neuroscience*, **44**(8), e0356232023.

Wollet, M., & Kim, J. H. (2022). Brain-derived neurotrophic factor is involved in activity-dependent tonotopic refinement of MNTB neurons. *Frontiers in Neural Circuits*, **16**, 784396.

Xiaoyu, W. (2015). The exposure to nicotine affects expression of brain-derived neurotrophic factor (BDNF) and nerve growth factor (NGF) in neonate rats. *Neurological Sciences*, **36**(2), 289–295.

Yao, W., & Godfrey, D. A. (1999). Immunolocalization of $\alpha 4$ and $\alpha 7$ subunits of nicotinic receptor in rat cochlear nucleus. *Hearing Research*, **128**(1–2), 97–102.

Zhang, C., Beebe, N. L., Schofield, B. R., Pecka, M., & Burger, R. M. (2021). Endogenous cholinergic signaling modulates sound-evoked responses of the medial nucleus of the trapezoid body. *Journal of Neuroscience*, **41**(4), 674–688.

Zhang, X., Liu, C., Miao, H., Gong, Z., & Nordberg, A. (1998). Postnatal changes of nicotinic acetylcholine receptor $\alpha 2$, $\alpha 3$, $\alpha 4$, $\alpha 7$ and $\beta 2$ subunits genes expression in rat brain. *International Journal of Developmental Neuroscience*, **16**(6), 507–518.

Zhong, C., Akmentin, W., Role, L. W., & Talmage, D. A. (2022). Axonal $\alpha 7^*$ nicotinic acetylcholine receptors modulate glutamatergic signaling and synaptic vesicle organization in ventral hippocampal projections. *Frontiers in Neural Circuits*, **16**, 978837.

Zhong, C., Du, C., Hancock, M., Mertz, M., Talmage, D. A., & Role, L. W. (2008). Presynaptic type III neuregulin 1 is required for sustained enhancement of hippocampal transmission by nicotine and for axonal targeting of $\alpha 7$ nicotinic acetylcholine receptors. *Journal of Neuroscience*, **28**(37), 9111–9116.

Additional information

Data availability statement

The data that support the findings of this study are available from the corresponding author upon reasonable request.

Competing interests

The authors declare no competing interests nor conflicts of interest.

Author contributions

M.W., J.H.K. and J.R.P. contributed to conception and design of the work. M.W., A.H., K.N., B.G., J.H.K. and J.R.P. contributed to acquisition, analysis or interpretation of data for the work. M.W., A.H., K.N., B.G., J.H.K. and J.R.P. contributed to drafting the work and revising critically for important intellectual content. All authors have approved the final version of the manuscript. All authors agree to be accountable for all aspects of the work. All persons designated as authors qualify for authorship, and all those who qualify for authorship are listed.

Funding

HHS | NIH | National Institute on Deafness and Other Communication Disorders (NIDCD): Mackenna Wollet F31DC021102.

HHS | NIH | National Institute on Deafness and Other Communication Disorders (NIDCD): Jun Hee Kim R01DC018797.

HHS | NIH | National Institute of Neurological Disorders and Stroke (NINDS): Jason R. Pugh R01NS123933.

Keywords

calyx of Held, development, nicotinic receptor, synaptic transmission

Supporting information

Additional supporting information can be found online in the Supporting Information section at the end of the HTML view of the article. Supporting information files available:

Peer Review History